

ANALYSIS AND DESIGN OF ACTIVE ANNULAR RING COUPLED
CIRCULAR PATCH ANTENNA

A THESIS SUBMITTED TO
THE GRADUATE SCHOOL OF NATURAL AND APPLIED SCIENCES
OF
MIDDLE EAST TECHNICAL UNIVERSITY

BY

DURMUŞ GEBEŞOĞLU

IN PARTIAL FULFILLMENT OF THE REQUIREMENTS
FOR
THE DEGREE OF MASTER OF SCIENCE
IN
ELECTRICAL AND ELECTRONICS ENGINEERING

APRIL 2017

Approval of the thesis:

**ANALYSIS AND DESIGN OF ACTIVE ANNULAR RING COUPLED
CIRCULAR PATCH ANTENNA**

submitted by **DURMUŞ GEBEŞOĞLU** in partial fulfillment of the requirements
for the degree of **Master of Science in Electrical and Electronics Engineering**
Department, Middle East Technical University by,

Prof. Dr. Gülbil Dural Ünver
Dean, Graduate School of **Natural and Applied Sciences** _____

Prof. Dr. Tolga Çiloğlu
Head of Department, **Electrical and Electronics Eng.** _____

Prof. Dr. S. Sencer Koç
Supervisor, **Electrical and Electronics Eng. Dept.,METU** _____

Examining Committee Members:

Prof. Dr. Özlem Aydin Çivi
Electrical and Electronics Eng. Dept.,METU _____

Prof. Dr. S. Sencer Koç
Electrical and Electronics Eng. Dept.,METU _____

Prof. Dr. Şimşek Demir
Electrical and Electronics Eng. Dept.,METU _____

Assoc. Prof. Dr. Lale Alatan
Electrical and Electronics Eng. Dept.,METU _____

Prof. Dr. Vakur B. Ertürk
Electrical and Electronics Eng. Dept.,Bilkent University _____

Date: 25.04.2017

I hereby declare that all information in this document has been obtained and presented in accordance with academic rules and ethical conduct. I also declare that, as required by these rules and conduct, I have fully cited and referenced all material and results that are not original to this work.

Name, Last name: DURMUŞ GEBEŞOĞLU

Signature:

ABSTRACT

ANALYSIS AND DESIGN OF ACTIVE ANNULAR RING COUPLED CIRCULAR PATCH ANTENNA

Gebeşoğlu, Durmuş

M. Sc., Department of Electrical and Electronics Engineering

Supervisor: Prof. Dr. S. Sencer Koç

April 2017, 94 pages

This thesis includes the design, production and measurement of the active, dual band annular ring coupled circular patch antenna. The dual band operation is achieved by using stacked patches. 3 dB hybrid is used to obtain circular polarization. Effects of antenna parameters on the input impedance and frequency ratio between the resonance frequencies are observed. Design has been achieved step by step. Firstly, dual band operation is investigated by using stacked patches. An annular ring antenna and a circular patch antenna are stacked to achieve dual band characteristic. Parametric analyzes are done in electromagnetic solver tool HFSS ®. The final antenna structure is revealed with parametric analyzes. After that, it is focused on to obtain circular polarization. 3 dB hybrid is designed in HFSS ®. The designed hybrid and antenna are combined. Circular polarization is realized by using 3 dB hybrid. At last, an attention is given to make the antenna active. Active circuit of the antenna is created in AWR Design Environment ®. The designed active dual band annular ring coupled circular patch antenna is manufactured and measured. The results of simulations and measurements are compared. Good agreements are observed between simulated and measured results.

KEYWORDS: Microstrip antennas, stacked patch antennas, active GPS antennas

ÖZ

AKTİF DAİRESEL HALKA KUPLAJLI DAİRESEL YAMA ANTEN ANALİZ VE TASARIMI

GEBEŞOĞLU, Durmuş

Yüksek Lisans, Elektrik ve Elektronik Mühendisliği Bölümü

Tez Yöneticisi: Prof. Dr. S. Sencer Koç

Nisan 2017, 94 sayfa

Bu tez, aktif, çift bant dairesel halka kuplajlı dairesel bir yama antenin tasarımını, üretimini ve ölçülmesini içerir. Çift bantta çalışabilme operasyonu yoğunlanmış yama antenlerle berhasilmıştır. Dairesel polarizasyon elde etmek için 3 dB hibrit kullanılmıştır. Tasarım aşamasında anten parametrelerinin giriş empedansı ve rezonans frekansları arasındaki frekans oranı üzerindeki etkileri gözlemlenmiştir. Tasarım kısmı adım adım geliştirilmiştir. İlk olarak yoğunlanmış yama antenlerle çift banta çalışabilme operasyonu incelenmiştir. Dairesel halka anten ve dairesel yama anten çift bantta çalışabilme karakteristiğini başarabilmek için birbiri üzerine yoğunlanmıştır. Parametrik analizler elektromanyetik çözümleyici yazılımı HFSS’te yapılmıştır. Parametrik analizlerle birlikte nihai anten yapısı ortaya çıkarılmıştır. Daha sonra dairesel polarizasyonu elde etmeye odaklanılmıştır. 3 dB hibrit HFSS’te tasarlanmıştır. Tasarlanan hibrit ve anten birleştirilmiştir. 3 dB hibritin kullanılmasıyla dairesel polarizasyon başarılı olmuştur. Antenin aktif devresi AWR tasarım ortamında oluşturulmuştur. Tasarlanan aktif, çift bantta çalışan, dairesel halka anten kuplajlı dairesel yama anten üretilmiştir. Simülasyon ve ölçüm sonuçları karşılaştırılmıştır. Ölçüm sonuçlarıyla simülasyon sonuçları arasında kabul edilebilir bir uyum elde edilmiştir.

ANAHTAR KELİMELER: Mikroşerit anten, yoğunlanmış yama antenler, aktif GPS antenleri

to my family

ACKNOWLEDGEMENTS

I would like to express my sincere gratitude to my advisor, Prof. Dr. Sencer Koç, for his guidance, support and technical suggestions throughout the study.

I would like to express my gratitude to Mustafa Kuloğlu providing invaluable support for both theoretical and practical topics throughout the study.

I am grateful to ASELSAN A.Ş. for the financial and technical opportunities provided for the completion of this thesis.

I would also like to express my sincere appreciation for Özkan Sağlam, Kadir İşeri Caner Asbaş and Akın Dalkılıç for their valuable friendship, motivation and help.

For their understanding my spending lots of time on this work, I sincerely thank to my wife Kamer Nur and my little daughter Elif Farah.

TABLE OF CONTENTS

ABSTRACT	v
ÖZ.....	vii
ACKNOWLEDGEMENTS	ix
TABLE OF CONTENTS	x
LIST OF TABLES	xiii
LIST OF FIGURES.....	xiv
FIGURES	xiv
CHAPTERS	
1. INTRODUCTION	1
2. MICROSTRIP PATCH ANTENNAS	15
2.1 Basic Design Considerations for Microstrip Patch Antennas	15
2.2 Analysis and Design of Circular Patch Antenna.....	16
2.2.1 Design Parameters of the Circular Patch Antenna	17
2.3 Analysis and Design of Annular Ring Antenna.....	19
3. DESIGN AND ANALYSIS OF ANNULAR RING COUPLED CIRCULAR PATCH ANTENNA.....	23
3.1 Circular Patch Antenna Design.....	24
3.2 Design and Analysis of Annular Ring Coupled Circular Patch Antenna	27
3.3 Parametric Analyzes of the Antenna.....	33
3.3.1 Effects of the Outer Radius of the Annular Ring Antenna	33
3.3.2 Effects of the Inner Radius of the Annular Ring Antenna	34
3.3.3 Effects of the Radius of Circular Patch Antenna	36

3.3.4	Effects of the Feed Position of the Antenna	37
3.3.5	Effect of the Thickness of the Bottom Substrate	39
3.3.6	Effects of the Top Substrate Thickness	40
3.3.7	Conclusions.....	42
4.	ANALYSIS and DESIGN of COUPLER	47
4.1	Analysis and Design of a Branchline Coupler.....	50
5.	AMPLIFYING CIRCUIT DESIGN.....	61
5.1	Introduction.....	61
5.2	Amplifying Circuit Design for GPS	64
5.2.1	Design of the Diplexer	66
6.	MANUFACTURING ACTIVE DUAL BAND ANNULAR RING COUPLED CIRCULAR PATCH ANTENNA AND MEASUREMENT RESULTS.....	75
7.	CONCLUSIONS	87
	REFERENCES.....	91

LIST OF TABLES

TABLES

Table 2.1 Roots of $J_n'(ka)=0$ [2]	18
Table 2.2 Roots for different b/a ratios [20].....	21
Table 3.1 Design parameters of the antenna	29
Table 3.2 Parameters and their effects on antenna performance.....	43
Table 3.3 Values of the parameters after tuning	44
Table 4.1 Power values at the coupler ports.....	53
Table 5.1 Comparison of the two topologies	64
Table 5.2 Element Values for Equal Ripple Low Pass Prototype.....	68
Table 5.3 Optimized Element Values	72

LIST OF FIGURES

FIGURES

Figure 1-1 Charge distribution on a microstrip antenna.....	3
Figure 1-2 Configuration of microstrip antennas [1]	3
Figure 1-3 Microstrip feed line [4].....	4
Figure 1-4 Proximity Coupled Feed [1]	4
Figure 1-5 Aperture Coupled Feed [1]	5
Figure 1-6 Electric Field Vector for Linear Polarization [7].....	6
Figure 1-7 Electric Field Vector for Elliptical Polarization [8]	7
Figure 1-8 Electric Field Vector for Circular Polarization [8].....	8
Figure 1-9 Axial ratio	9
Figure 1-10Single fed circularly polarized patch antennas;	10
Figure 1-11 Double feed patch antennas	10
Figure 1-12 Multipath problems due to structural reflections [9]	11
Figure 2-1 Higher order mode radiation pattern of the circular patch [2].....	18
Figure 2-2 Geometry of an annular ring antenna [2].....	20
Figure 3.1 Structure of the circular patch antenna	24
Figure 3.2 Return loss of the patch (radius=26.4 mm).....	25
Figure 3.3 Return loss of the patch (radius=25.8 mm).....	26
Figure 3.4 Axial ratio of the patch (radius=25.8 mm)	27
Figure 3.5 The structure of annular ring coupled circular patch antenna.....	28
Figure 3.6 Return loss of the stacked patch and circular patch ($R_{cp}=25.8$ mm, $R_{innerAr}=17$ mm, $R_{outerAr}=35.7$ mm, $H1=2$ mm, $H2=1$ mm).....	30
Figure 3.7 Input impedances of the stacked patch and circular patch.....	30
Figure 3.8 Current distribution for annular ring antenna (For 1227 MHz)	31
Figure 3.9 Current distribution of the circular patch antenna (For 1575 MHz).....	31
Figure 3.10 3D radiation pattern for 1227 MHz	32
Figure 3.11 3D radiation pattern for 1575 MHz	32

Figure 3.12 Return loss for different radius	33
Figure 3.13 Input impedances for different radius	34
Figure 3.14 Return loss for different inner radius	35
Figure 3.15 Input impedances for different inner radius.....	35
Figure 3.16 Effect of different circular patch radius on return loss	36
Figure 3.17 Effect of different circular patch radius on input impedance	37
Figure 3.18 Effect of the feed distance on the return loss.....	38
Figure 3.19 Effect of the feed distance on the input impedance	39
Figure 3.20 Effect of the bottom substrate thickness on the return loss	39
Figure 3.21 Effect of the bottom substrate thickness on the input impedance.....	40
Figure 3.22 Effect of the top substrate thickness on the return loss.....	41
Figure 3.23 Effect of the top substrate thickness on the input impedance.....	42
Figure 3.24 Return loss of the antenna after fine tuning.....	44
Figure 3.25 RHCP directivity of the antenna at 1227 MHz.....	45
Figure 3.26 RHCP directivity of the antenna at 1590 MHz.....	45
Figure 4.1 General directional coupler symbol.....	47
Figure 4.2 Basic branchline coupler [21]	50
Figure 4.3 Unequal branchline coupler [22]	50
Figure 4.4 Normalized form of the branchline coupler [21]	51
Figure 4.5 (a) even mode excitation, (b) odd mode excitation [21].....	51
Figure 4.6 Determining the thicknesses of the transmission lines in HFSS	54
Figure 4.7 stripline coupler geometry (a) top view, (b) side view	55
Figure 4.8 S parameters of the stripline coupler	56
Figure 4.9 Phase of the through and coupled ports	56
Figure 4.10 E field distribution on the upper ground plane	57
Figure 4.11 Coupler with shorting screws	58
Figure 4.12 E field distribution on the upper ground plane	58
Figure 4.13 S parameters of the coupler with shorting screws	59
Figure 4.14 Phase of the through and coupled ports	59

Figure 5.1 GPS antenna system with RF filter and LNA	62
Figure 5.2 GPS antenna system with LNA, RF filter and LNA.....	62
Figure 5.3 T junction simulation model	65
Figure 5.4 S parameters of the T junction	65
Figure 5.5 Configuration of the diplexer.....	66
Figure 5.6 Prototype beginning a series element [30].....	67
Figure 5.7 Attenuation versus normalized frequency for equal ripple filters [30]..	67
Figure 5.8 Diplexer circuit with lumped elements	71
Figure 5.9 S parameters of the Diplexer.....	72
Figure 5.10 Schematic of the active circuit.....	73
Figure 5.11 S parameters of the Active Circuit.....	74
Figure 6.1 Fabrication of the antenna.....	76
Figure 6.2 Return loss comparison with fabricated and simulated antenna.....	76
Figure 6.3 Fabricated antenna	77
Figure 6.4 Optimized return loss of the antenna	78
Figure 6.5 S parameters of the stripline coupler	78
Figure 6.6 Phase of the stripline coupler	79
Figure 6.7 Fabricated stripline coupler.....	80
Figure 6.8 Fabricated Active Circuit.....	80
Figure 6.9 S parameters of the active circuit.....	81
Figure 6.10 SATIMO Near Field Measurement System.....	82
Figure 6.11 Placement of the antenna in SATIMO	82
Figure 6.12 Axial ratio of the lower band (GPS L2).....	83
Figure 6.13 Axial ratio of the upper band (GPS L1 and GLONASS L1)	83
Figure 6.14 Radiation pattern of the antenna at 1227 MHz	84
Figure 6.15 Radiation pattern of the antenna at 1575 MHz	84
Figure 6.16 Radiation pattern of the antenna at 1605 MHz	85
Figure 6.17 Frequency dependent gain of the antenna.....	85

CHAPTER 1

INTRODUCTION

Global Positioning System (GPS) is a system that can be used to locate any positions on the world. GPS is an American System which was developed in 1978. GPS was developed for U.S Military needs firstly. Afterwards, the system is made available for civilians [5]. In addition to GPS, there are similar systems in use. The Russian Global Navigation Satellite System (GNSS) is one of the other positioning systems. GPS and GNSS are very similar systems with small differences. The main difference between GPS and GNSS is coverage. GPS system has better coverage at low and mid latitudes where most of world's population lives. However, GNSS has better coverage at high latitudes. At last decade, many devices are developed for using these two systems together to improve the accuracy or to determine the position faster. There are also lots of positioning systems in the world. We will focus on GPS and GNSS systems in this thesis. GPS requires dual or multi frequency operations. The aim of this study is to design a circularly polarized, active GPS antenna which works at GPS L1 (1575.42 MHz), GPS L2 (1227.60 MHz) and GLONASS L1 (1602 MHz) frequencies. The design consists of three main parts. First step is to design of an annular ring coupled circular patch antenna. The second step is to design a branch line coupler that provides 90 degree phase difference to manage circular polarization. The third part of the design is an active circuit that comprise of band pass filter and low noise amplifier (LNA).

In some applications where size, cost, ease of installations are required, low profile antennas such as microstrip antennas can be used [1]. Microstrip antennas are one

of the most attractive antennas because of their low cost, low profile and easy for fabrication. They are also known as printed circuit antennas and are often used as conformal antennas.

Basically microstrip antennas comprise of a very thin patch ($t \ll \lambda_0$, λ_0 is the free space wavelength) where printed on a thin dielectric material ($h \ll \lambda_0$) [1]. Dielectric material used in the antenna generally has dielectric constant lower than 10 ($\epsilon_r < 10$, ϵ_r is the dielectric constant) [2] to enhance the fringing fields that account for the radiation. Some other performance requirements may also affect the choice of dielectric material such as width of transmission lines, power handling of the antenna, size of the antenna etc. In GPS applications there is no necessity of high power handling of the antenna since the antenna is used for receiving purposes. Therefore high power handling is not a constraint in the design of GPS antennas. However, demanding lower size of the GPS antenna has effect on the choice of dielectric material. Generally high dielectric constant materials like ceramic are used as the substrate in order to reduce the size of the GPS antennas. Cost of the material is another reason for preference. FR-4 material is used in many applications due to lower cost than the others. As microstrip antennas have only a substrate and a metal, patch antennas can be produced at a low cost depending on the choice of substrate.

Although there are lots of advantages of microstrip antennas, they have also some disadvantages. The most significant disadvantage of the microstrip antennas is narrow impedance bandwidth. Additionally, they have also low gain and low power handling capability.

The radiation of the microstrip antennas is generated by the field distribution between the patch and ground plane. When the patch is excited, a charge distribution on the upper and lower surfaces of the patch is created as can be seen from Figure 1.1.

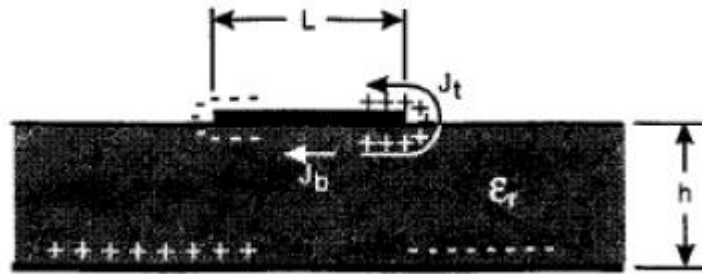


Figure 1-1 Charge distribution on a microstrip antenna

There are lots of feeding techniques to excite the microstrip antennas. All feeding methods have some advantages and disadvantages. Selection of feeding technique is the most important factor for efficient power transfer to the antenna.

Coaxial feeding is one of the most popular feeding techniques. Basically, the inner conductor of the coaxial cable is soldered to the patch and the outer conductor of the coaxial cable is soldered to the ground plane of the microstrip antenna [3] [Figure 1-2]. The position of the feed is important in this technique as it controls the input impedance of the antenna. Coaxial feeding may cause matching problems when substrate is thick due to inductive loading on the input impedance. Impedance of a microstrip antenna feeding with this technique is suitable for matching along a narrow bandwidth.

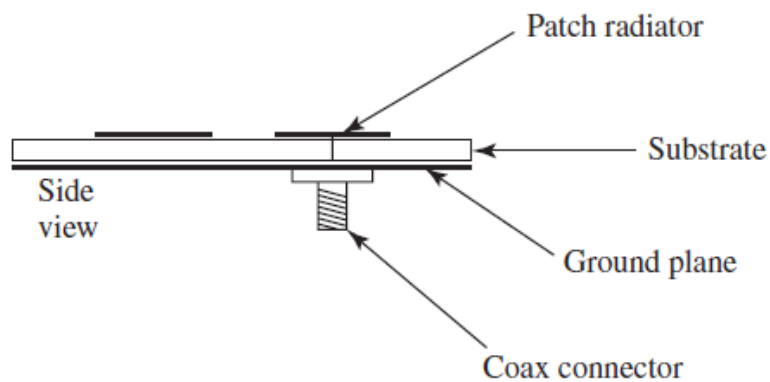


Figure 1-2 Configuration of microstrip antennas [1]

Microstrip antennas may also be excited by a microstrip line. This method is the most basic method to feed the antenna as the microstrip line and antenna on the same layer of the substrate. Microstrip line can be considered as an extension of the microstrip antenna [Figure 1-3]. To match the antenna, microstrip line inset cut can be used. The disadvantage of the microstrip line feed is that as substrate thickness increases, the impedance bandwidth is limited due to surface wave and spurious feed radiation increases [1].

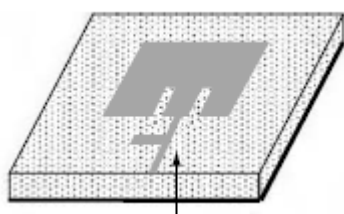


Figure 1-3 Microstrip feed line [4]

One of other feed techniques for microstrip antennas is proximity (electromagnetically) coupled feed. Proximity coupled feed needs two dielectric substrates. Patch is on the upper substrate while microstrip feed line is between the substrates as shown in Figure 1-4. The ground plane is below the lower substrate. This is also a non-touching method because the power is coupled from the microstrip feed line to the radiating patch. The open end of the microstrip feed line can be terminated by a stub to obtain a better matching. The parameters of the two substrates such as dielectric constant and thicknesses can be optimized to increase the bandwidth of the antenna.

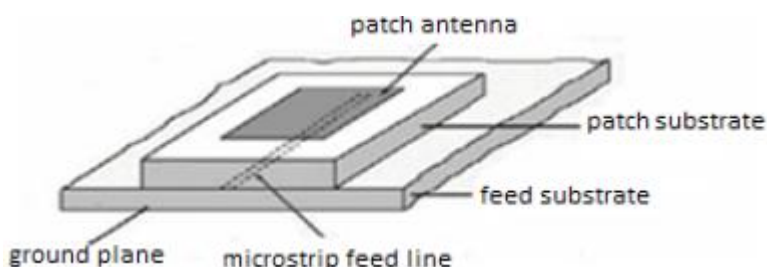


Figure 1-4 Proximity Coupled Feed [1]

One of the most used feed techniques for microstrip antennas is aperture coupled feeding. This feed technique comprise of two dielectric substrates with a ground plane between substrates. On the lower substrate, there is a microstrip line to feed the antenna through a slot on the ground plane. Various shapes may be used for slot to improve the impedance bandwidth of the antenna. Radiating patch antenna is positioned on the upper substrate. Dielectric constants and thicknesses of the substrates, width of the feed line, shape of the slot and shape of the radiating patch are the parameters that control the impedance bandwidth. The disadvantage of this method is difficulty in fabrication. Figure 1-5 shows the aperture coupled feed.

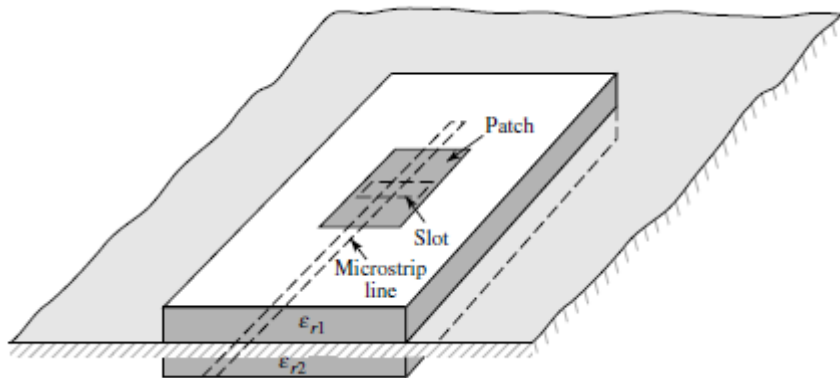


Figure 1-5 Aperture Coupled Feed [1]

One important parameter for an antenna is polarization. “*The polarization of a wave is the direction of the electric field with respect to time*” [6]. It is possible to say that movement of the electric field that is radiated by the antenna in space determines the polarization of the antenna. It is very important to match the antenna polarization with the signal that comes to the antenna. In this manner the maximum signal is received. Otherwise, there may be a dramatic decrease in the signal strength.

The polarization of the antenna may be linear, circular and elliptic. The basic forms of polarization are vertical and horizontal polarizations. They are both categorized as linear polarization. “*If the vector that describes the electric field at a point in*

space as a function of time is always directed along a line, the field is said to be linearly polarized. In general, however, the figure that the electric field traces is an ellipse, and the field is said to be elliptically polarized. Linear and circular polarizations are special cases of elliptical, and they can be obtained when the ellipse becomes a straight line or a circle, respectively” [1].

When the electric field is oriented always along the same straight line, the polarization of this wave is linear. Monopole and dipole antennas are examples of linearly polarized antennas. These antennas may also be used for both vertical and horizontal polarization by positioning them vertically or horizontally. Figure 1-6 shows the electric field vector for linearly polarized antennas.

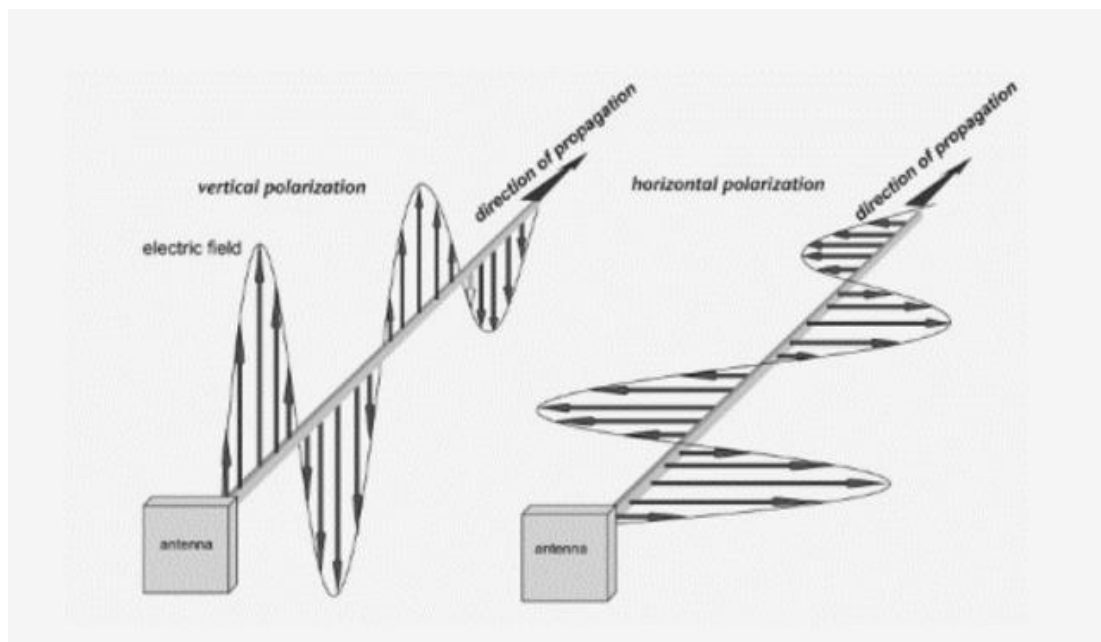


Figure 1-6 Electric Field Vector for Linear Polarization 0

Any electric field can be decomposed into two orthogonal linearly polarized waves.

If the E field is decomposed into two orthogonal components:

$$E = E_x \cos(\omega t - \beta z) \vec{a}_x + E_y \cos(\omega t - \beta z + \phi) \vec{a}_y \quad (1.1)$$

At a fixed position ($z=0$), equation (1.1) can be written as

$$E = E_x \vec{a}_x + E_y \cos(\omega t + \phi) \vec{a}_y \quad (1.2)$$

An antenna is linearly polarized, if θ is equal to $n\pi$ where $n=0,1,2\dots$ in equation (1.2). An antenna is elliptically polarized if the radiated electric field vector traces an ellipse. The amplitude of the components that is perpendicular to each other may be same or different for elliptical polarization. There are two conditions for elliptical polarization. If these two components do not have the same magnitude, θ should not be 0° or multiples of 180° . Otherwise, it is linearly polarized. If they have the same magnitude, θ should not be odd multiples of 90° , because it will have circular polarization in this situation. There are two types of elliptical polarization. If electric field vector rotates clockwise regarding to direction of propagation, it is right hand elliptically polarized and if electric field vector rotates counter-clockwise regarding to direction of propagation then it is left hand elliptically polarized. Figure 1-7 shows the electric field vector for elliptical polarization.

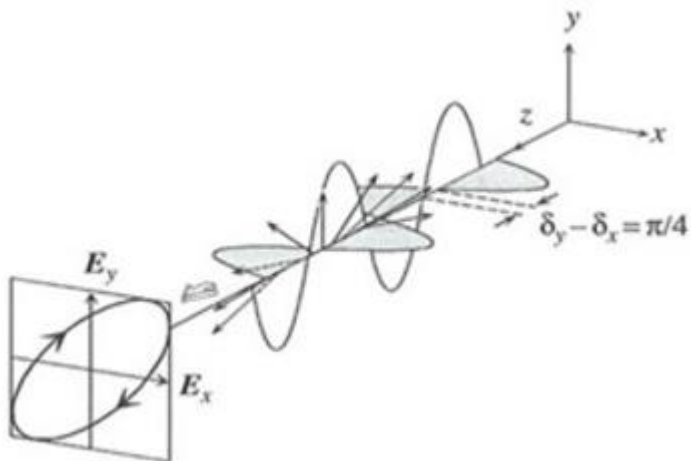


Figure 1-7 Electric Field Vector for Elliptical Polarization [8]

Circular polarization is a special case of elliptical polarization. An antenna is circularly polarized if the radiated electric field vector traces is a circle as a function of the time. The electric field can be decomposed two orthogonal linear components like elliptical polarization. These two orthogonal field components must have same magnitude and θ should be the odd multiples of 90° . There are two

types of circular polarization like elliptical polarization. If electric field vector rotates clockwise with reference to direction of propagation, it is right hand circularly polarized and if electric field vector rotates counter-clockwise then it is left hand circularly polarized. Figure 1-8 shows the electric field vector trace for circular polarization.

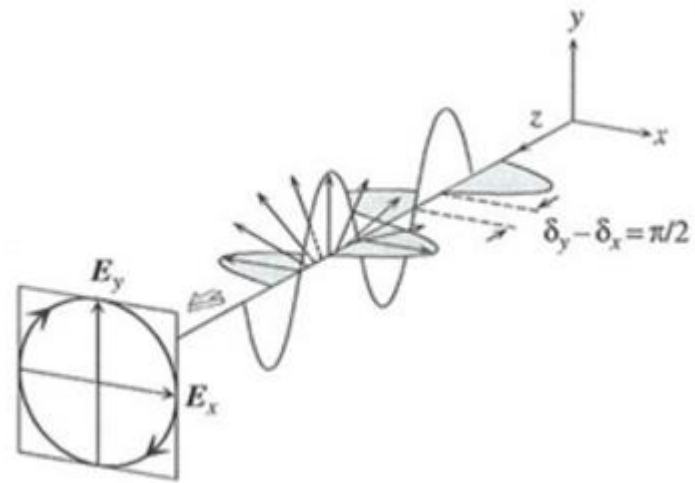


Figure 1-8 Electric Field Vector for Circular Polarization [8]

One important parameter for the antennas is axial ratio. Figure 1.9 shows the polarization ellipse. Axial ratio is the ratio ($AR=a/b$) of major axis and minor axis of the ellipse which is the trace of electric field movement in time (Figure 1-9).

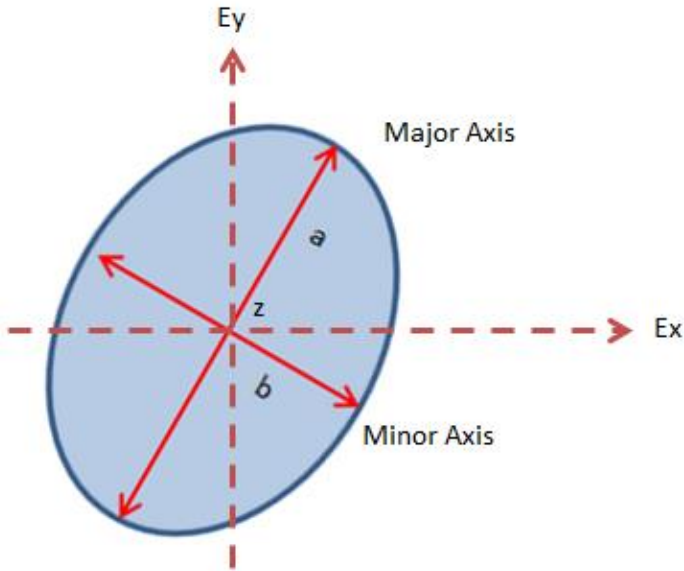


Figure 1-9 Axial ratio

The axial ratio of the linearly polarized antennas is infinite ($AR=\infty$), since the minor axis of the ellipse is zero. A circularly polarized wave has equal major and minor components that gives the $AR=1$. For elliptically polarized waves major and minor components are not equal in magnitude that gives $1 < AR < \infty$. Axial ratio is an important parameter for antennas in literature. In many design, the axial ratio should be lower than 3 dB in frequency band for circular polarization. Some antennas have circular polarization in nature of their structure as spiral antennas, helical antennas etc. Since microstrip antennas are linearly polarized, additional methods should be implemented in order to achieve circular polarization. “*For a circular polarized radiation, a patch must support orthogonal fields of equal amplitude but in-phase quadrature*” [2]. There are lots of methods to get circular polarization for patch antennas.

Circular polarization can be achieved by exciting two orthogonal modes in equal amplitude and $\pm 90^\circ$ out of phase for a patch antenna. The sign of phase difference indicates the sense of polarization i.e, RHCP or LHCP. The methods of obtaining circular polarization for single feed and double feed antennas are different. Orthogonal patch modes can be excited by using perturbation techniques in single

feed antennas. It is easy to fabricate single feed antennas but, the main disadvantage of this method is narrow axial ratio bandwidth [12]. Figure 1-10 shows the feeding of patch antennas with single excitation point to get circular polarization by perturbation techniques.

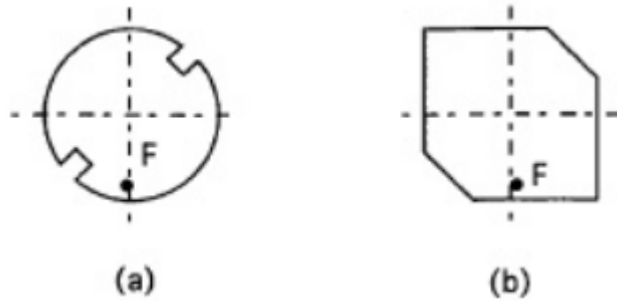


Figure 1-10 Single fed circularly polarized patch antennas;

(a) Circular patch and (b) Square Patch [2]

Another technique to obtain circular polarization for patch antennas is obtained by using double feed points to excite orthogonal modes directly in the antenna. In this method, there should be also a power divider which provides equal amplitude and $\pm 90^\circ$ phase difference for two feeding points. Quadrature hybrids are used in literature for circular polarization generally. This method has wider axial ratio bandwidth than perturbation techniques. Figure 1-11 shows double feed patch antennas to get circular polarization.

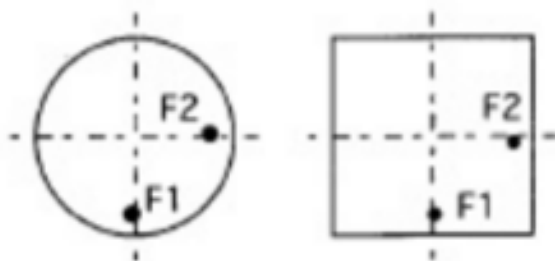


Figure 1-11 Double feed patch antennas

(a) Circular patch and (b) Square patch [2]

Circular polarization is used in many radio systems like radars, communication systems and satellite systems. There are many advantages of usage of circular polarization in systems. Especially in satellite systems where electromagnetic waves come from far away, electromagnetic waves may not be received by the receiver antenna due to polarization mismatch. Antennas which radiate and/or receive circularly polarized waves may radiate and/or receive both vertical and horizontal polarization waves also. This situation is the advantage of circular polarization since it decreases polarization mismatch. Due to these advantages, circular polarization is used for GPS antennas too. GPS satellites radiate RHCP waves; for this reason, GPS antennas in ground systems should receive RHCP waves. Structural reflections sometimes may change RHCP waves to LHCP waves. In some applications it is necessary to reject cross polarized waves [9].

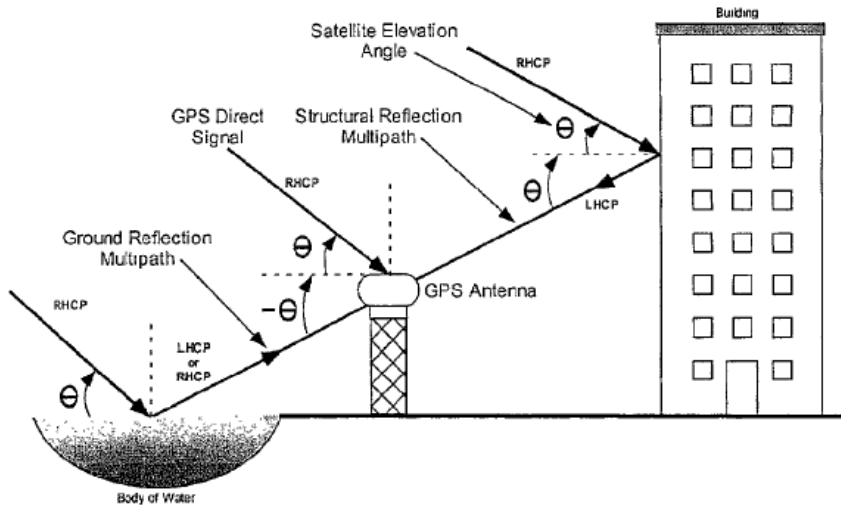


Figure 1-12 Multipath problems due to structural reflections [9]

Dual band, circularly polarized microstrip antennas are studied in the literature before. The main problems are generally narrow impedance bandwidth and narrow axial ratio bandwidth. In [14] and [15] thicker substrates are used to enhance impedance bandwidth. Stacked structure is studied by Rod in [10]. It is specified that the choice of substrate in stacked structures is very important since it controls the impedance behavior of the antenna. The structure is studied for three antenna

element types, circular patch, square patch and annular ring patch antenna. %25 impedance bandwidth is achieved with the thickness of the substrates $0.04 \lambda_0$ and $0.06 \lambda_0$. For GPS frequencies these thicknesses are quite large.

A dual band circularly polarized stacked annular ring patch antenna is presented in [11]. Antenna operates at both L1 and L2 frequencies of GPS. Circular polarization is achieved by a 3dB hybrid. Aperture coupled feeding technique is used in this design and H shape slot is preferred for aperture.

In [12], it is specified that stacked patch antennas which consist of a lower substrate with high dielectric constant and an upper substrate with low dielectric constant substrate have low cross polarization. “*It is important to note that the main source of cross polarized fields is the discontinuity associated with the feed and the driven patch conductor. This is why direct contact fed patches have greater cross-polarization levels than noncontact printed antennas (such as aperture-coupled patches)*” [13].

The main aim of this thesis is to design a circularly polarized, active GPS antenna which works at GPS L1, L2 and GLONASS L1 frequencies. Since, GPS L1 (1575.42 MHz) and GLONASS L1 (1602 MHz) frequencies are close to each other, same microstrip patch antenna element is used for these frequencies. For GPS L2 frequency, different microstrip antenna element is used. The stacked patch configuration is used to obtain dual band operation. Circular patch antenna is excited by double coaxial probes. Annular ring antenna is excited by parasitically coupling from circular patch antenna. Parametric analyzes are done to investigate the effects of the parameters on the input impedance of the antenna. External 3 dB coupler is necessary to obtain circular polarization in order to excitation of orthogonal modes on the patch. Various coupler types are studied. Branchline coupler is used to enhance circular polarization. The last design process of the antenna is to make the antenna active. Active GPS antennas are researched in the

literature. Active circuit of the antenna is designed by using AWR design environment. The designed active annular ring coupled circular patch antenna is manufactured and measured. The results of simulations and measurements are compared.

CHAPTER 2

MICROSTRIP PATCH ANTENNAS

Microstrip patch antennas consist of a patch radiator on one side of dielectric and a ground plane on the other side of the dielectric. Various shape of microstrip patches are used for microstrip antennas such as rectangular, circular, annular etc. Rectangular and circular patch antennas are widely preferred. They all have same radiation characteristics in spite of the differences of their shapes. In this thesis stacked annular ring coupled circular patch antenna is studied. Circular patch antenna is used on the bottom substrate while the annular ring antenna is used on the top patch. In this study, the annular ring antenna is preferred for the top patch, due to size of the annular ring antenna is relatively smaller than the circular and rectangular patch antennas for a given frequency. This chapter explains the design consideration of circular patch and annular ring antenna.

2.1 Basic Design Considerations for Microstrip Patch Antennas

As stated before, microstrip antennas can be designed in any shape, with some limitations such as dielectric constant of the substrate, thickness of the substrate, size of the ground plane and feeding point etc. All these parameters affect the antenna's electrical properties such as return loss, gain, pattern etc. Choosing the best substrate is the first and important step of the design. Substrates that can be used in antennas have dielectric constants usually in a range $2.2 \leq \epsilon_r \leq 12$ [1]. Thicker substrates that have lower dielectric constants are the most preferred because they increase the efficiency and bandwidth. Disadvantage of the thicker substrates are larger size and dielectric loss. Lower value of ϵ_r will increase the

fringing field, so the radiated fields will increase. Disadvantage of lower ϵ_r is the larger patch size. In some applications large value of ϵ_r is preferred to minimize the antenna size.

Another important parameter of the microstrip antennas is the feed location. Feed location affects the input impedance of the antenna. Matching of the antenna can be done easily by changing the location of the feed. Feed location can also affect the polarization of the antennas especially in single feed antennas. Circular polarization can be achieved by determining the feed location on the diagonal of the antenna in single feed nearly square patch antenna.

2.2 Analysis and Design of Circular Patch Antenna

Circular patch antenna is one of the most preferred patch antennas along with the rectangular patch antenna. Circular patch antenna is relatively smaller than the rectangular patch antenna [2]. In some designs, circular geometries are more suitable over alternative patches. Circular patch antenna is analyzed with various methods such as transmission line model [16], [17] mode matching with edge admittance [18] and cavity model [2]. The cavity model is analyzed as follows [2]:

Circular patch antenna can be modeled as a cylindrical cavity and electric fields in the cavity should satisfy equation (2.1) along with boundary condition.

$$(\nabla^2 + k^2)\vec{E} = 0 \quad (2.1)$$

$$k = 2\pi\sqrt{\epsilon_r}/\lambda_0 \quad (2.2)$$

The solution of this wave equation is;

$$E_z = E_0 J_n(k\rho) \cos(n\phi) \quad (2.3)$$

Where J_n is the Bessel function of order n . At this point we can define X_{nm} that is the m th zero of the $J_n(k\rho)$. The resonance will occur if $ka=X_{nm}$, where $n=0,1,2\dots$ and $m=1,2,3\dots$. In this equation ‘ a ’ denotes the radius of the circular patch. We can easily calculate the radius of the circular patch antenna at resonance frequency as;

$$a = \frac{X_{nm}}{k} \quad (2.4)$$

The fundamental mode of the circular disk antenna can be obtained if the values of n and m are equal to 1. Minimum patch radius for a given frequency can be obtained at the dominant mode.

2.2.1 Design Parameters of the Circular Patch Antenna

To design a circular patch antenna, some parameters should be determined such as substrate, radius of the patch, radiation pattern etc. In this section we will study these important parameters.

First step of the design is choosing a suitable substrate. Lower dielectric constant substrates are preferred generally, for better radiation efficiency. Thickness of the substrate affects the bandwidth of the antenna. Thicker substrates have larger bandwidth. Second step of the design is determining the radius of the patch antenna. As stated before the radius of the patch can be calculated using equation (2.4). If we modify the equation (2.4), it will transform to equation (2.5).

$$f_{nm} = \frac{X_{nm}c}{(2\pi a_e \sqrt{\epsilon_r})} \quad (2.5)$$

Where ‘ a_e ’ is the effective radius of the patch antenna,

‘c’ is the speed of light in free space,

‘ f_{nm} ’ is the resonance frequency,

‘ ϵ_r ’ is the effective dielectric constant of the substrate

‘ X_{nm} ’ is the root of characteristic equation

Some lower order modes are given in Table 2.1.

Table 2.1 Roots of $J_n'(ka)=0$ [2]

Mode(n,m)	0,1	1,1	2,1	0,2	3,1	4,1	1,2
Root X_{nm} or $k_{nm}a$	0	1.84118	3.05424	3.83171	4.20119	5.317	5.331

An effective radius is introduced in equation (2.5). For the dominant mode (TM_{11}), it is suggested in [2], to calculate the effective radius of the circular patch ;

$$a_e = a \left\{ 1 + \frac{2h}{\pi a \epsilon_r} \left(\ln \left(\frac{\pi a}{2h} \right) + 1.7726 \right) \right\}^{0.5} \quad (2.6)$$

Radiation patterns of the circular patch are obtained in [2] by using cavity model, these expressions are shown below;

$$E_\theta = -\frac{jVak_0}{2} \frac{e^{-jk_0r}}{r} \cos\theta J'_1(k_0 a \sin\theta) \quad (2.7)$$

$$E_\phi = \frac{jVak_0}{2} \frac{e^{-jk_0r}}{r} \frac{J_1(k_0 a \sin\theta)}{k_0 a \sin\theta} \cos\theta \sin\phi \quad (2.8)$$

Where $V = hE_1 J_1(k_{nm}a)$ is the edge voltages at $\phi=0$.

Radiation pattern of the circular patch antenna is obtained in broadside for fundamental (TM_{11}) mode. In some applications such as satellite systems, it may be necessary to use conical patterns with a null in broadside. Conical pattern may be obtained if the patch antenna is excited in a higher mode. Higher order mode radiation patterns of the circular patch antenna are shown in figure 2-1.

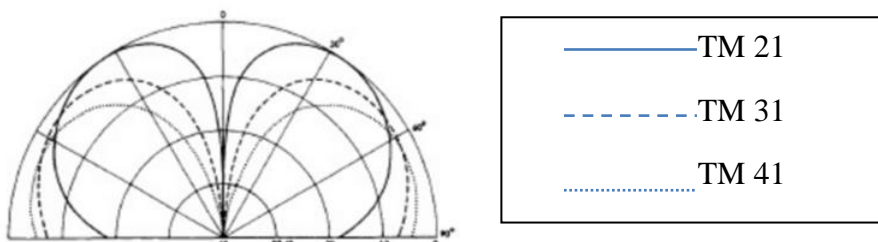


Figure 2-1 Radiation patterns of the higher order modes of circular patch [2]

Radiated power may be calculated by using (2.7) and (2.8) in equation (2.9);

$$P_r = (1/2\eta_0) \int_0^{2\pi} \int_0^{\pi/2} (E_\theta^2 + E_\phi^2) r^2 \sin\theta d\theta d\phi \quad (2.9)$$

Location of the feed point is another design parameter for circular patch antenna. After selecting a dielectric substrate and determining the radius of the patch, location of the feed should be determined. Feeding location affects the impedance of the antenna, so good matching depends on the location of the feed. Feeding point distance depends on the radiation resistance and Bessel Function. The input impedance of the antenna can be calculated;

$$R_{in} = R_r \frac{J_1^2(k_{11}r_0)}{J_1^2(k_{11}a)} \quad (2.10)$$

where,

‘ R_{in} ’ is the input impedance of the antenna

$$‘R_r’ \text{ is the radiation resistance which is equal to } R_r = \frac{(E_0 h)^2}{2P_r} \quad (2.11)$$

‘ J_1 ’ is the Bessel Function,

‘ r_0 ’ is the feeding point distance from the center of the antenna,

‘ a ’ is the radius of the antenna,

‘ k_{11} ’ is equal to $\frac{x_{11}}{a}$

2.3 Analysis and Design of Annular Ring Antenna

Annular ring antennas are alternatives to both rectangular and circular patch antennas. There are lots of shapes of annular ring antenna such as circular, rectangular, triangular etc. The advantage of the annular ring antenna is the smaller size of the antenna than rectangular and circular patch antenna for a given resonance frequency. Dominant mode is TM_{11} . In this mode, the real part of the input impedance of the antenna is very large, so the bandwidth of the antenna is

smaller than circular patch at a given resonance frequency. When the width of the annular ring increases, the characteristics of the antenna will be similar to circular patch antenna.

The impedance bandwidth of the antenna can be very large, if the antenna is excited in TM_{12} mode. The disadvantage of this mode is larger size. Annular ring antenna may also be analyzed with cavity model. The general wave equation solution which is obtained by cavity model for a given coordinate system shown in Figure 2-2 is given in [2];

$$E_z = E_0 [J_n(k\rho)Y'_n(ka) - J'_n(ka)Y_n(k\rho)] \cos(n\phi) \quad (2.12)$$

$$H_\rho = \frac{j}{\omega\mu\rho} \frac{dE_z}{d\phi} \quad (2.13)$$

$$H_\phi = -\frac{j}{\omega\mu} \frac{dE_z}{d\rho} \quad (2.14)$$

where J_n and Y_n are the Bessel functions of first and second kind, and of order n . Other field components are zero in the cavity.

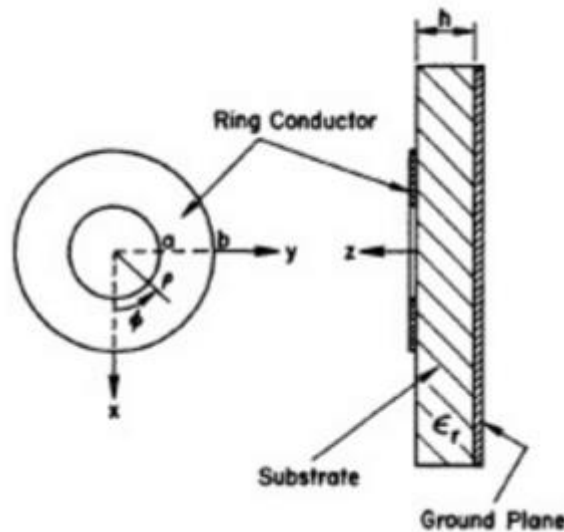


Figure 2-2 Geometry of an annular ring antenna [2]

To satisfy the magnetic boundary conditions, surface current on the lower edges goes to zero.

$$J_p(\rho=a)=H_\phi(\rho=a)=0 \text{ and } J_p(\rho=b)=H_\phi(\rho=b)=0 \quad (2.15)$$

Using equations (2.15), below characteristic equation is obtained for resonant condition.

$$J'_n(kb)Y'_n(ka)-J'_n(ka)Y'_n(kb)=0 \quad (2.16)$$

The roots of equation (2.16) which may be denoted by X_{nm} , define the resonant frequencies of annular ring antenna. ‘n’ denotes the azimuthal variation while m denotes the mth zero of the above equation. As stated for circular patch antenna, TM₁₁ mode has also the minimum radius for a given frequency and is known as dominant mode. Some of the roots are given in Table 2.2 for different b/a ratios.

Table 2.2 Roots for different b/a ratios [20]

$\chi_{nm} = k_{nm}a$	TM11	TM12	TM13
$b/a = 2.1$	0.656586	3.00369	5.78542
$b/a = 2.3$	0.618632	2.5761	4.91264
$b/a = 2.5$	0.584713	2.26364	4.2733
$b/a = 2.7$	0.554172	2.02534	3.7849
$b/a = 2.8$	0.540007	1.92619	3.58156

An approximate value is obtained by cavity model for the inner radius of the annular ring antenna [2];

$$a = \frac{X_{nm}c}{2\pi f \sqrt{\epsilon_r}} \quad (2.17)$$

Where,

‘ X_{nm} ’ is the roots of characteristic equation,

‘c’ is the speed of light,

‘f’ is the frequency,

‘ ϵ_r ’ is the dielectric constant

In above equation fringing field effect is not accounted. If we use effective dielectric constant in the above equation, we can increase the accuracy.

$$a = \frac{X_{nm}c}{2\pi f \sqrt{\epsilon_r}} \quad (2.18)$$

Radiation field calculation of the annular ring antenna is similar with circular patch antenna. The difference is that there are two magnetic current sources for annular ring antenna. Radiation fields at $\rho=a$ and $\rho=b$ are calculated independently and added vectorial to obtain annular ring antenna. Radiated fields are obtained in [2];

$$E_0 = j^n \frac{2E_0}{\pi k_{nm}} \frac{e^{-jk_0r}}{r} k_0 h [J_n(k_0 a \sin \theta) - \frac{J'_n(k_{nm}a)}{J'_n(k_{nm}b)} J_n(k_0 b \sin \theta)] \cos(n\phi) \quad (2.19)$$

$$E_\phi = -nj^n \frac{2E_0}{\pi k_{nm}} \frac{e^{-jk_0r}}{r} k_0 h \left[\frac{J_n(k_0 a \sin \theta)}{k_0 a \sin \theta} - \frac{\frac{J'_n(k_{nm}a)}{J'_n(k_{nm}b)} J_n(k_0 b \sin \theta)}{k_0 b \sin \theta} \right] \sin(n\phi) \cos \theta \quad (2.20)$$

$$\text{where, } k_{nm} = \frac{x_{nm}}{a}$$

CHAPTER 3

DESIGN AND ANALYSIS OF ANNULAR RING COUPLED CIRCULAR PATCH ANTENNA

In this chapter, an annular ring coupled circular patch antenna is investigated to get dual band, circularly polarized characteristic. Dual band characteristic is obtained by using two different antenna element type. Circular patch antenna is designed for GPS L1 (1575.42 MHz) and GLONASS L1 (1602 MHz) frequencies and annular ring antenna is designed for GPS L2 (1227.60 MHz) frequency. The design step starts with substrate selection of the circular patch antenna. Because of the low cost properties, FR4 substrate is chosen for the circular patch antenna. Single band circular patch antenna is designed. All analysis are done in HFSS (High Frequency Structural Simulator) ® commercial software. After that, it is focused on to get dual band characteristic. Dual band characteristic is provided with an extra antenna element that is an annular ring. The reason to choose annular ring is size minimization. Annular ring antenna has lower size than both circular patch and rectangular patch for a given frequency at the cost of smaller bandwidth. Since GPS L2 band is very narrow, annular ring antenna provides sufficient bandwidth. Dual band, annular ring coupled circular patch antenna is studied in this chapter. Parametric analyzes are done.

3.1 Circular Patch Antenna Design

The first step is the design of the circular patch antenna. In this section, the design of circular patch antenna is studied and its parameters are investigated. FR4 substrate is chosen for the design. The radius of the patch is determined first using the equations discussed in chapter 2 and optimized with simulations for the desired resonance frequency.

$$a_e = \frac{X_{11c}}{2\pi f \sqrt{\epsilon_r}} \quad (3.1)$$

where,

$X_{11}=1.84118$ is the first root of the derivative of Bessel Function of order one for dominant mode of the circular patch antenna,

‘c’ is the speed of light that value is 2.98×10^8 m/s,

‘ ϵ_r ’ is the 4.4 for FR4 substrate,

‘f’ is chosen as 1590 MHz which is between GPS L1 (1575.42 MHz) and GLONASS L1 (1602 MHz) frequencies.

With these parameters the radius of the patch is calculated approximately as 26.4 mm. The simulations are started with this initial value. The structure of the circular patch is shown in Figure 3.1.



Figure 3.1 Structure of the circular patch antenna

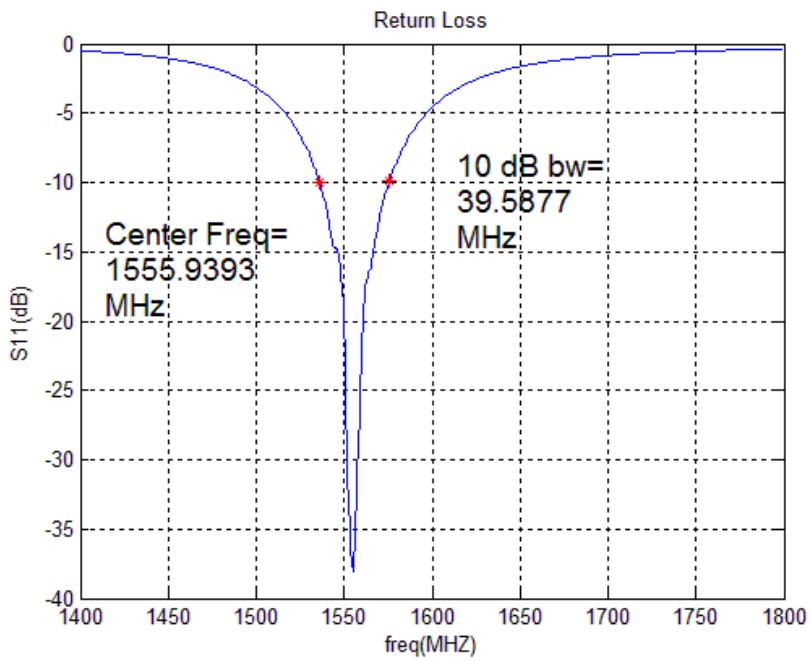


Figure 3.2 Return loss of the patch (radius=26.4 mm)

The return loss of the patch that has a radius of 26.4 mm is shown in Figure 3.2. The center frequency is 1555 MHz, so the resonance frequency is shifted by approximately 35 MHz. The reason of the shift is probably related to the thickness of the substrate. Simulations are started with the 1.524 mm FR4 substrate. Radius of the patch is optimized to give resonance frequency 1590 MHz. 25.8 mm radius is obtained with the simulations to achieve the resonance frequency. The return loss of the patch that has the radius 25.8 mm is given in Figure 3.3.

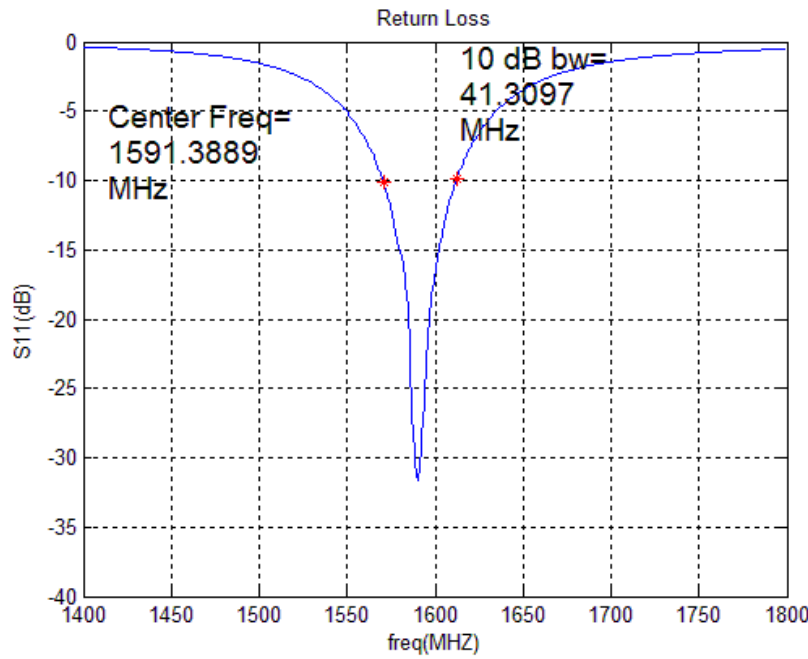


Figure 3.3 Return loss of the patch (radius=25.8 mm)

GPS L1 and GLONASS L1 frequencies are achieved with the radius 25.8 mm on the 1.524 mm FR4 substrate. In all analysis, circular patch antenna is fed by two points. These two points are fed with wave ports in HFSS. Wave ports are excited with 90 degree phase difference to obtain circular polarization. Axial ratio characteristic is shown in Figure 3.4. Due to perfect 90 degree phase shift between the two ports, axial ratio of the antenna is very good. After this step, design of a dual band antenna is studied.

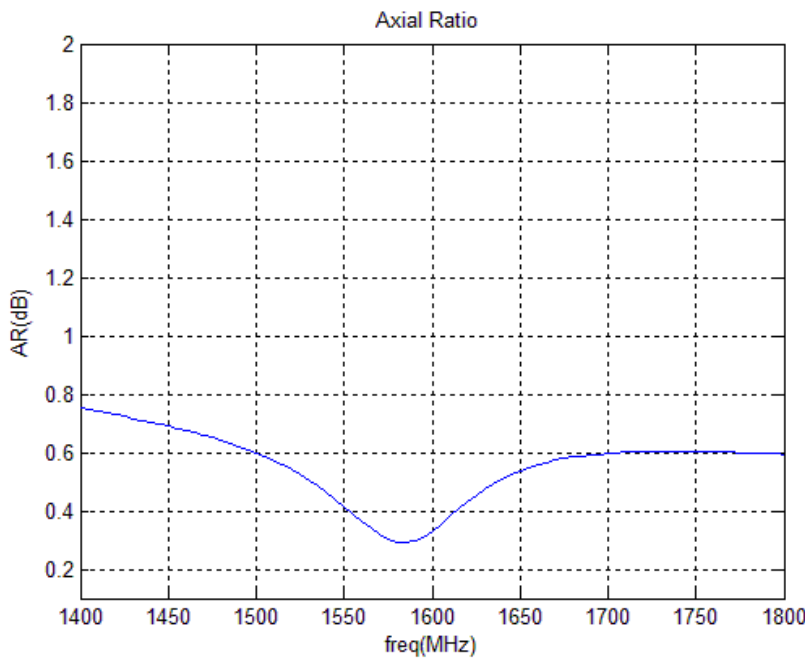


Figure 3.4 Axial ratio of the patch (radius=25.8 mm)

3.2 Design and Analysis of Annular Ring Coupled Circular Patch Antenna

Dual band characteristic can be achieved by using an extra antenna element. In previous studies, stacked patch antennas are used for dual band GPS antennas. In this study, annular ring antenna and circular patch antenna are stacked to achieve dual band characteristic. The reason of the choice of annular ring antenna element is smaller size with respect to circular patch antenna with the cost of narrow bandwidth. Since GPS L2 band is narrow, annular ring antenna can be used for this band. The design starts by calculating the inner and outer radius of the annular ring antenna. It is stated that combination of the high dielectric constant and low dielectric constant substrates have good impedance behavior [10] in stacked patch antennas. FR4 substrate is chosen for circular patch and Rogers 5880 substrate is chosen for annular ring antenna. For the dominant TM₁₁ mode, the inner radius of the annular ring antenna for 1227 MHz is calculated using the following formula.

$$a = \frac{X_{11}c}{2\pi f \sqrt{\epsilon_r}} \quad (3.2)$$

where,

$X_{11} = 0.656586$ is root of the characteristic equation for the b/a ratio is 2.1.

$c = 2.98 * 10^8$ is the speed of light,

$f=1227.60$ MHz is the center frequency of GPS L2 band,

$\epsilon_r=2.2$ is the dielectric constant of Rogers 5880 substrate.

Inner radius of the annular ring antenna is calculated about 17 mm using above values. Annular ring coupled circular patch antenna structure is shown in Figure 3.5.

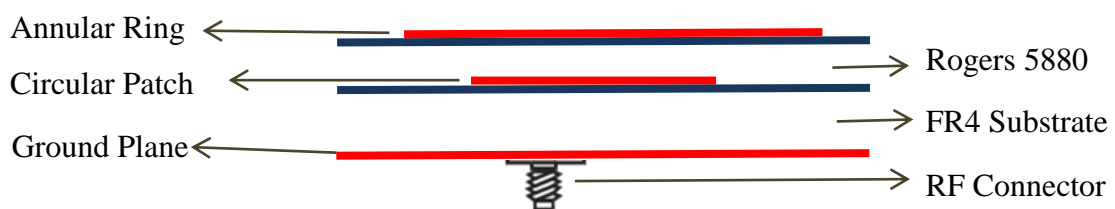


Figure 3.5 The structure of annular ring coupled circular patch antenna

During the design process, many parameters should be investigated such as the radius of the antennas, thickness of the substrates, feeding points etc. All these parameters are shown in Table 3.1.

Table 3.1 Design parameters of the antenna

Name of the Parameter	Definition of the Parameter
R_outerAr	Outer radius of the annular ring
R_innerAr	Inner radius of the annular ring
R_cp	Radius of the circular patch
H1	Thickness of the lower substrate
H2	Thickness of the upper substrate
L_feed	Distance of the feed from the center

In section 3.1, circular patch antenna is designed with the parameters that are $h1=1.524$ mm and $R_{cp}=25.8$ mm on the FR4 substrate. In this section, design is started with these parameters and also annular ring antenna is added to the design to obtain dual band characteristic. Rogers 5880 material is chosen for upper substrate that has the dielectric constant 2.2. In the first design, the parameter H2 is chosen as 1mm and $R_{innerAr}$ is calculated 17mm by using equation (3.2). The first root of the characteristic equation in (2.16) is chosen for the ratio of $R_{outerAr}$ to $R_{innerAr}$ 2.1. So, $R_{outerAr}$ is calculated as 35.7 mm. The return loss characteristic of the design is shown in Figure 3.6.

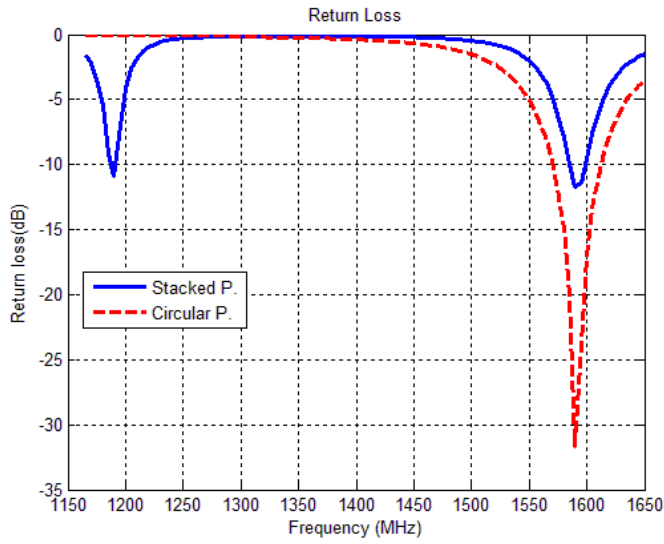


Figure 3.6 Return loss of the stacked patch and circular patch ($R_{cp}=25.8$ mm,
 $R_{innerAr}=17$ mm, $R_{outerAr}=35.7$ mm, $H1=2$ mm, $H2=1$ mm)

The wide band characteristic of the circular patch becomes narrower with the addition of annular ring as shown in Figure 3.6. The reason for this situation is shown in Figure 3.7. The real part of the input impedance increases with the addition of the annular ring antenna and also imaginary part becomes sharper in upper band.

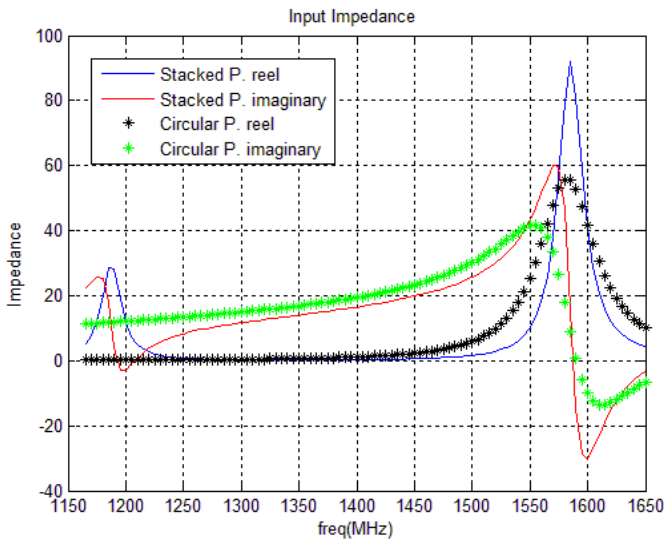


Figure 3.7 Input impedances of the stacked patch and circular patch

The fast variation of the input impedance limits the impedance bandwidth in upper band. The lower band resonance occurs due to the presence of annular ring antenna element. In the next section, studies to obtain wider bandwidth through parametric analyzes are given.

TM_{11} mode is used for both circular patch and annular ring antenna. When the circular patch is fed by two orthogonal feeds having same amplitude and a phase difference of 90 degrees the current distributions on the antennas are shown in Figure 3.8 and Figure 3.9.

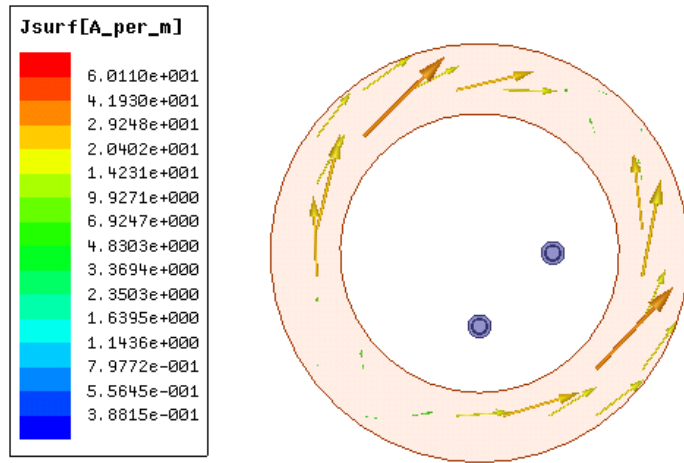


Figure 3.8 Current distribution for annular ring antenna (For 1227 MHz)

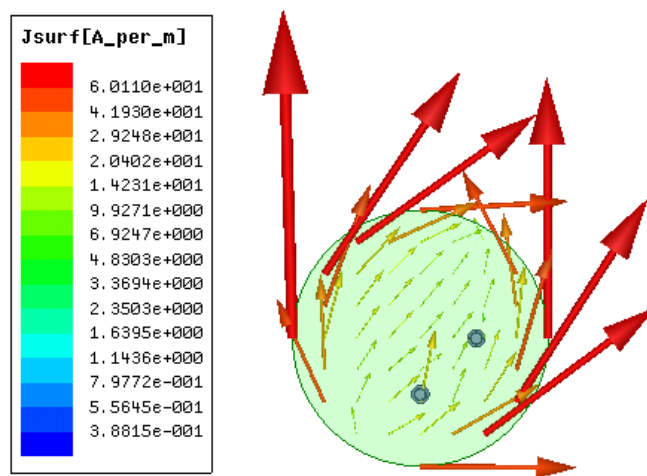


Figure 3.9 Current distribution of the circular patch antenna (For 1575 MHz)

Directivity characteristics are shown in Figure 3.10 and Figure 3.11. Peak directivity of the antenna at both lower and upper resonance are in the broadside direction ($\theta=0^\circ$).

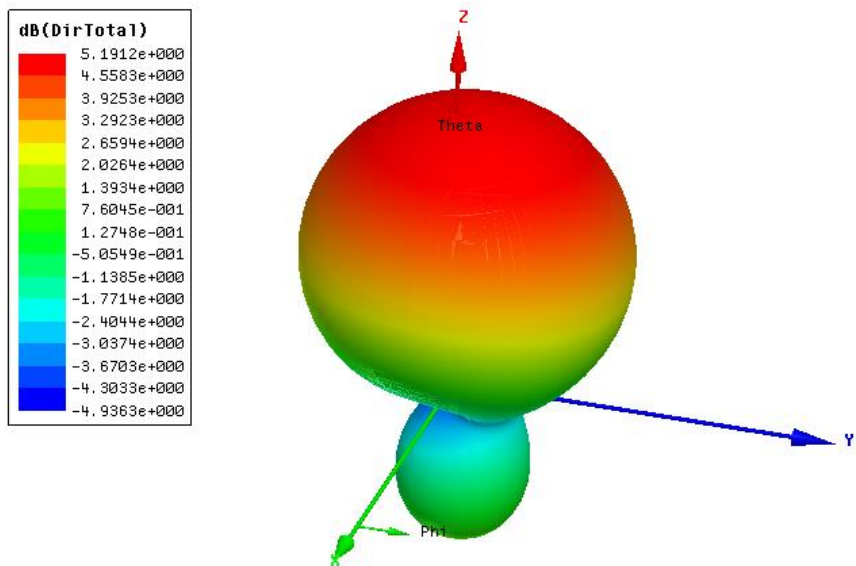


Figure 3.10 3D radiation pattern for 1227 MHz

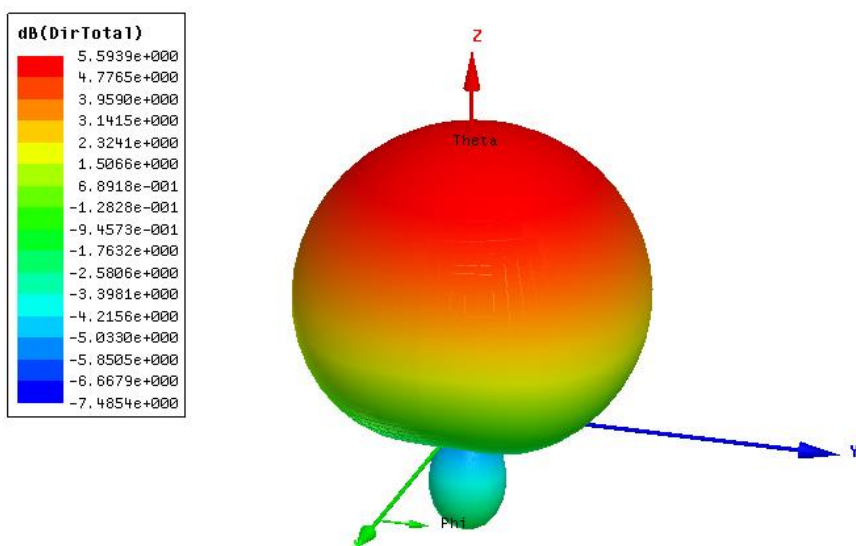


Figure 3.11 3D radiation pattern for 1575 MHz

3.3 Parametric Analyzes of the Antenna

In this section, antenna parameters are tabulated in Table 3.1, namely outer radius of the annular ring, inner radius of the annular ring, radius of the circular patch, feed point of the antenna, thicknesses of the substrates are studied.

3.3.1 Effects of the Outer Radius of the Annular Ring Antenna

The first investigated parameter is the outer radius of the annular ring antenna. Effects of changing the outer radius of the annular ring on the input impedance are investigated in this section. The parameter $R_{outerAr}$ is changed between 29 mm and 31 mm while other parameters are constant. Results of this analysis are shown in Figure 3.12 and the effect of this parameter on the input impedance is shown in Figure 3.13.

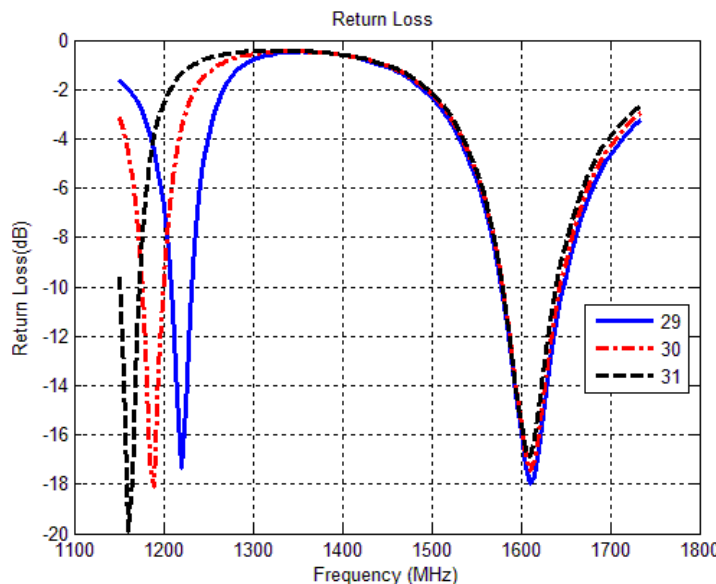


Figure 3.12 Return loss for different radius

As it can be seen from Figure 3.12, changing outer radius of the annular ring does not affect the upper resonance. In addition Figure 3.12 shows that, when the outer radius of the annular ring increases, the lower resonance frequency decreases.

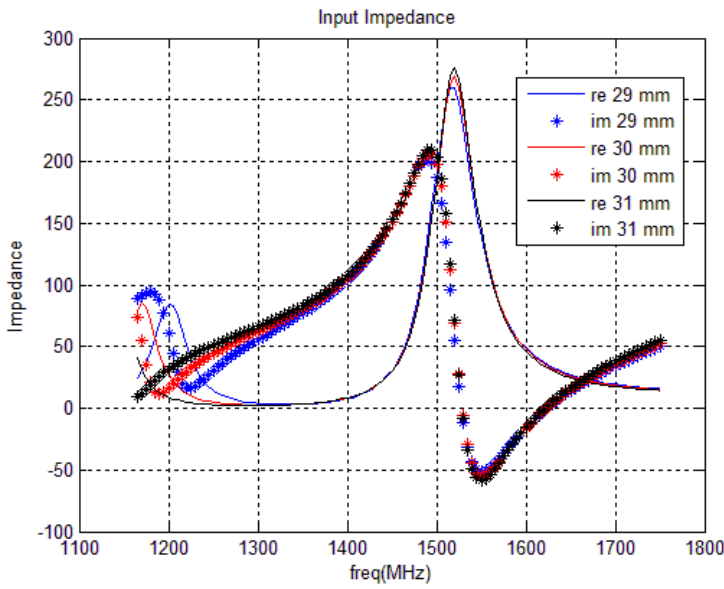


Figure 3.13 Input impedances for different radius

As it can be seen in Figure 3.13, the real and imaginary parts of the input impedance shifts with changing outer radius in lower band, but upper band is not affected from this change. This parameter significantly affects the frequency ratio between the two resonances.

3.3.2 Effects of the Inner Radius of the Annular Ring Antenna

In this section, effects of the inner radius of the annular ring on return loss and bandwidth are investigated. The parameter $R_{innerAr}$ is changed between 18 mm and 22 mm while other parameters are constant. Changing the return loss of the antenna is shown in Figure 3.14. As it can be seen from Figure 3.14, changing inner radius of the annular ring affects both upper and lower bands. Increasing the inner radius of the annular ring, increases the upper resonance bandwidth while decreases the lower resonance bandwidth.

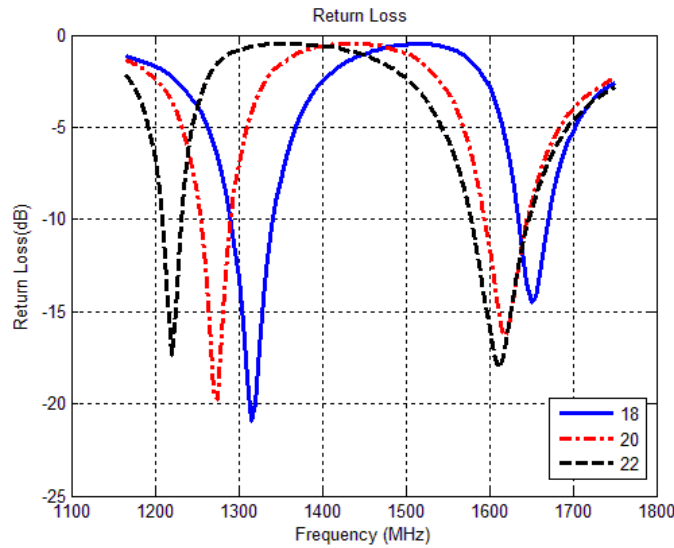


Figure 3.14 Return loss for different inner radius

As it can be seen from Figure 3.15, increasing the inner radius decreases the real part of the input impedance well below 50 ohm in the lower resonance frequency as width of the annular ring is reduced. On the other hand increasing values of this parameter, increase the upper resonance bandwidth due to decreasing the capacitance between the annular ring and circular patch antennas.

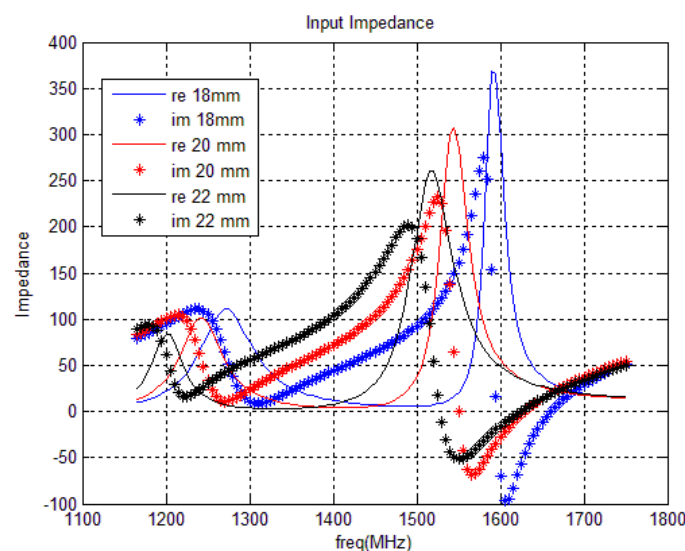


Figure 3.15 Input impedances for different inner radius

As it can be seen from Figure 3.15, increasing inner radius, decreases the resonance frequency for both band.

3.3.3 Effects of the Radius of Circular Patch Antenna

In this section, the effects of the radius of the circular patch on the impedance characteristic of the antenna are studied. Parameter R_{cp} is changed between 23.5 mm and 24.5 mm while other parameters are kept constant. This parameter affects the lower resonance slightly while it changes the upper resonance frequency significantly. Radius of the circular patch mainly determines the resonance frequency of the upper band. Changing the radius also affects the lower resonance due to the change in capacitance between the annular ring and circular patch. Return loss characteristic is shown in Figure 3.16.

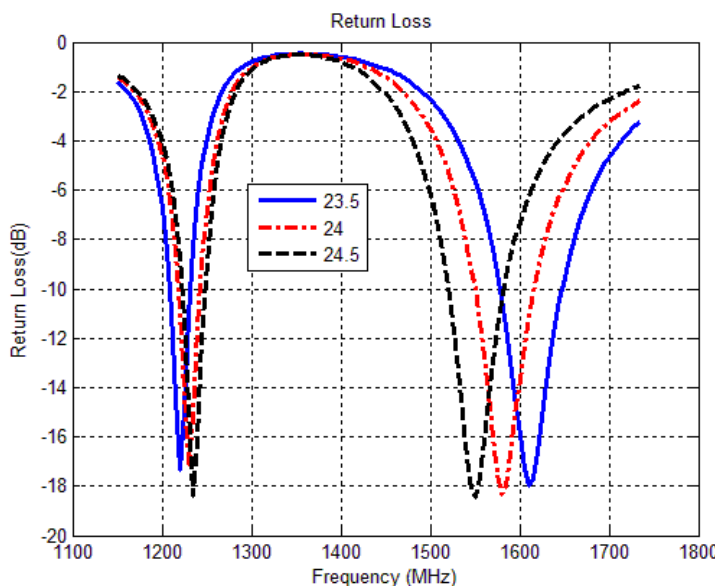


Figure 3.16 Effect of different circular patch radius on return loss

As it can be seen from the Figure 3.16, the resonance frequency of the upper band decreases when the radius of the circular patch increases. Figure 3.17 shows the input impedance of the antenna for different radii. It can be said that, slight changes in the reactance part of the impedance for lower frequency affects the return loss slightly.

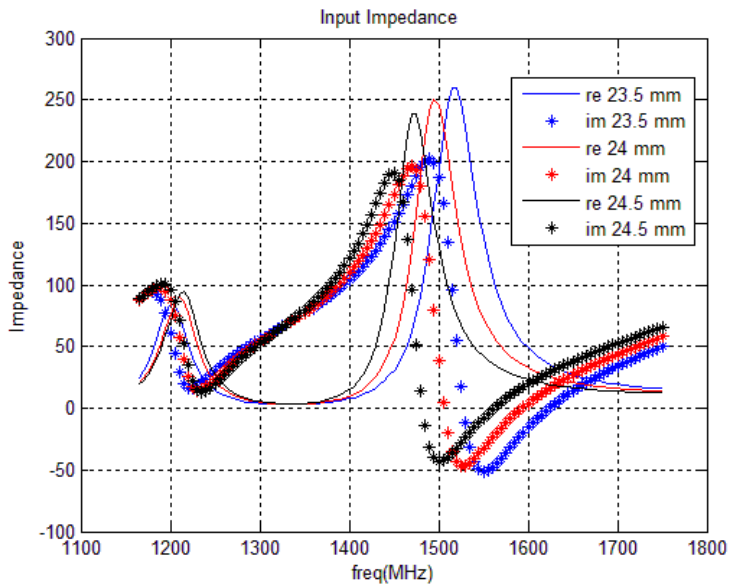


Figure 3.17 Effect of different circular patch radius on input impedance

3.3.4 Effects of the Feed Position of the Antenna

One of the most important parameters that affects the input impedance of the antenna is feed position. Coaxial feeding is used to feed the antenna. The parameter L_{feed} is defined as the distance from the center of the patch and parametric analyzes are done. L_{feed} is changed between 11.5 mm and 13 mm. The return loss characteristic of the antenna is shown in Figure 3.18. Changing the feed position slightly affects the resonance frequency for both bands but has significant effects on the depth of the return loss. As it can be seen from Figure 3.18, when the feed distance from the center of the circular patch increases, the upper band return loss gets worse in contrast to lower band. Lower band return loss gets better when the feed distance increases.

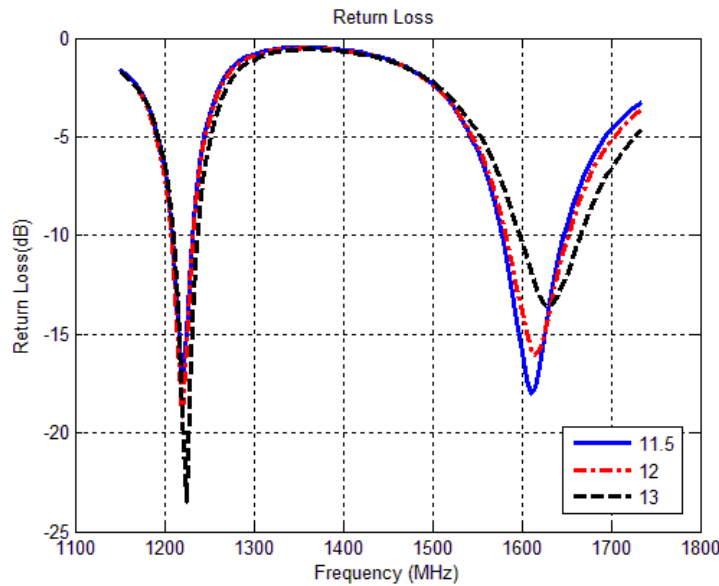


Figure 3.18 Effect of the feed distance on the return loss

The input impedance is shown in Figure 3.19. As can be seen from Figure 3.19, if the feed point of the antenna moves away from the center of the patch the input impedance of the antenna will be more capacitive. Upper resonance is affected negatively due to decrease in depth of the return loss. On the other hand, real part of impedance for the lower band is approaching to 50 ohm and the imaginary part of the input impedance approaches the 0 for the lower resonance. Lower resonance is affected positively due to increase in the depth of the return loss. Choice of this parameter may cause a trade-off between the two resonances.

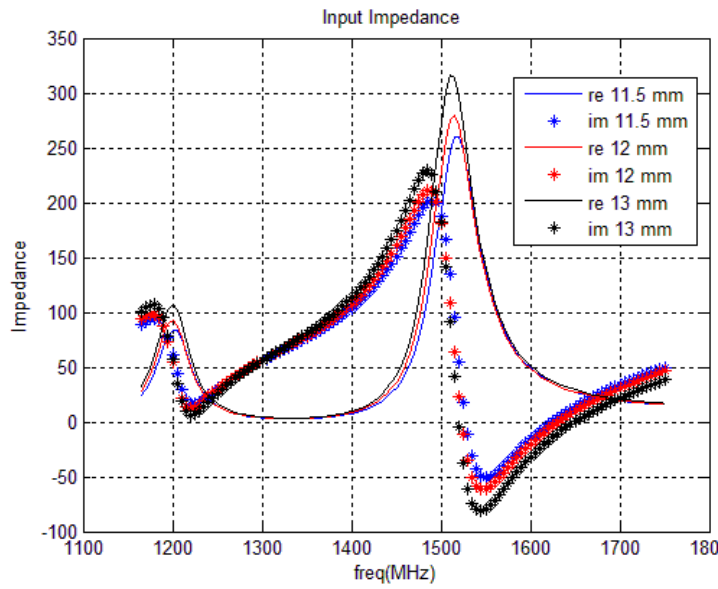


Figure 3.19 Effect of the feed distance on the input impedance

3.3.5 Effect of the Thickness of the Bottom Substrate

This section includes the effects of the thickness of the bottom substrate on return loss characteristic of the antenna. Parametric analyses is done by changing the substrate thickness from 6mm to 8mm. Return loss is given in Figure 3.20.

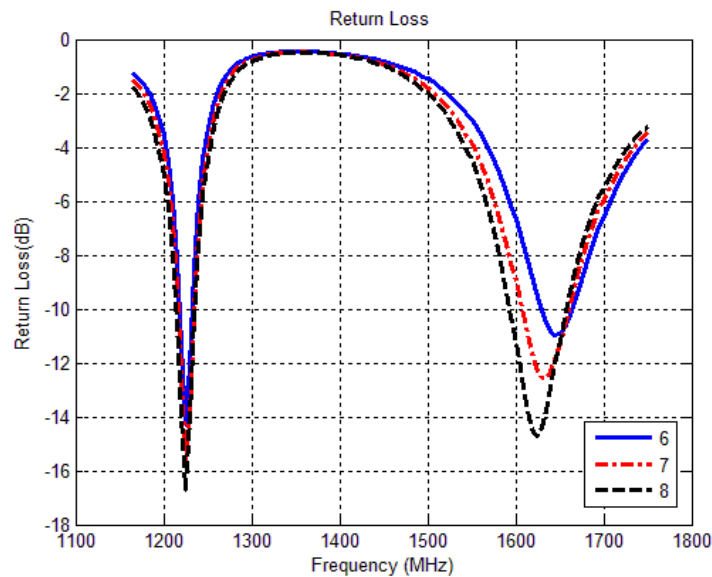


Figure 3.20 Effect of the bottom substrate thickness on the return loss

It is observed from Figure 3.20 that upper resonance frequency shifts with increasing the thickness of the substrate. Figure 3.21 shows the variation of input impedance by changing thicknesses.

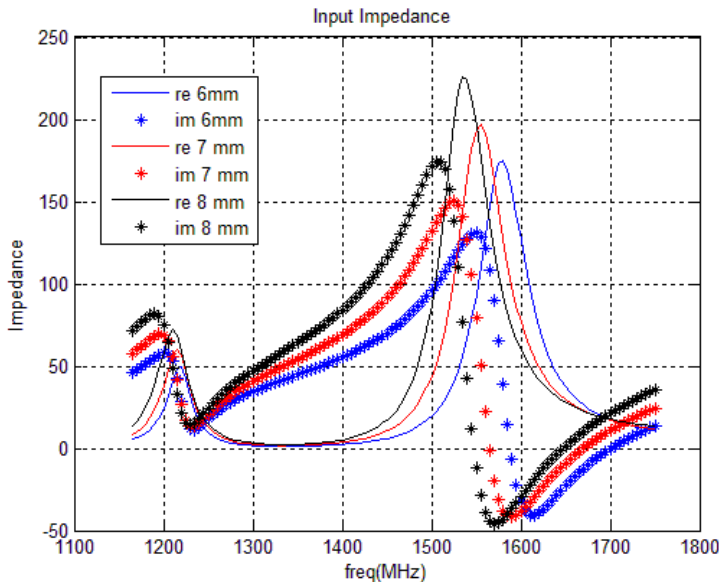


Figure 3.21 Effect of the bottom substrate thickness on the input impedance

As it can be seen from Figure 3.21, real part of the input impedance increases as the thickness of the substrate increases and also the span of the imaginary part of the impedance gets larger. Imaginary part of the impedance has an inductive behavior due to an increase in the coaxial probe length. This parameter has important effect on the impedance bandwidth for both upper and lower resonance. With changing the thickness, other parameters are also affected due to variation of the electrical length. As it can be seen from return loss graph, an important parameter for the larger bandwidth is thickness of the substrate. All other parameters are optimized after the optimization of thickness.

3.3.6 Effects of the Top Substrate Thickness

Thickness of the top substrate is an important parameter that has significant effects on the impedance bandwidth for both bands. Parametric analysis of the top substrate thickness is given in this section. Thickness of the substrate is changed

between 0.5mm and 2mm. All other parameters are constant during parametric analysis. Figure 3.22 shows the return loss characteristic of the antenna.

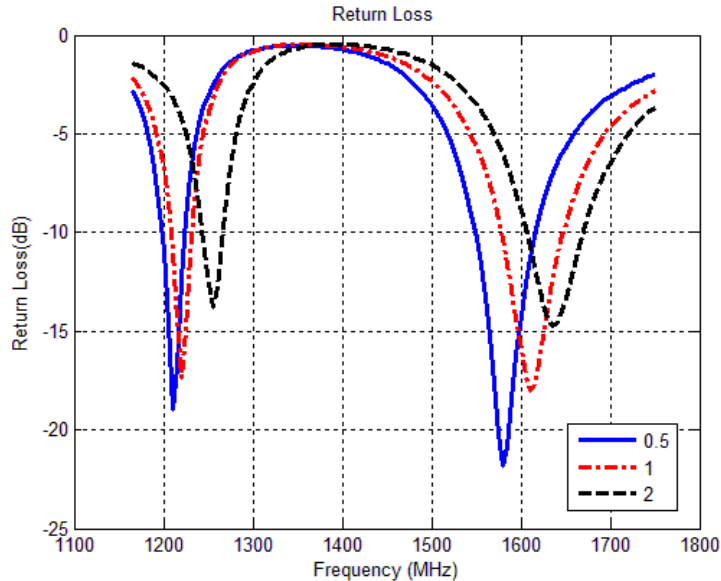


Figure 3.22 Effect of the top substrate thickness on the return loss

This parameter is related with the coupling between the antennas. Decreasing values of this parameter, increase the coupling between the antennas. As it can be seen from Figure 3.22, increasing the top substrate thickness, increases the resonance frequency for both bands. Reduction in upper resonance bandwidth can be observed in Figure 3.23. With increasing thickness, real part of the impedance increases and imaginary part of the impedance gets sharper for upper band. In this case it causes the bandwidth to decrease. For the lower band, this parameter generally affects the resonance frequency, not the impedance bandwidth.

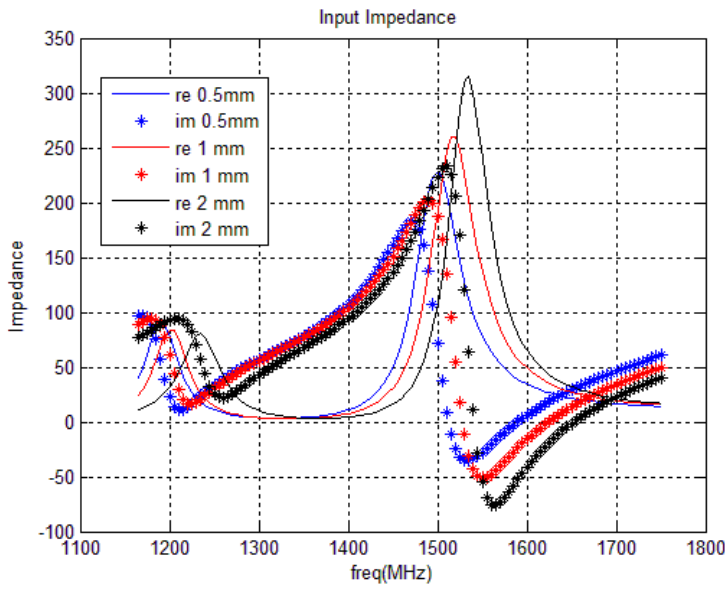


Figure 3.23 Effect of the top substrate thickness on the input impedance

3.3.7 Conclusions

All of these analyzes were performed to obtain a bandwidth covering the frequencies of GPS L1, GPS L2 and GLONASS L1. The effects of important design parameters that are given in Table 3.1 are analyzed. Table 3.2 is obtained as a result of these analyzes. Radii of the patches affect the frequency ratio significantly. All other parameters have slight effect on the frequency ratio. All parameters affect the resonance frequency. The most important parameters for the impedance bandwidth are thicknesses of the substrates. Feeding point location can be used to tune the return loss of the antenna. Table 3.2 summarizes the parameters and their effects on the antenna performance.

Table 3.2 Parameters and their effects on antenna performance

	Design Parameters (Increasing values)					
	R_outerAr	R_innerAr	R_cp	H1	H2	L_feed
Resonance Frequency For Lower Band	↓	↓	✗	↓	↑	✗
Resonance Frequency For Upper Band	✗	↓	↓	↓	↑	✗
Return Loss	✓	✓	✓	✓	✓	✓
Frequency Ratio	↑	↑ (Slightly)	↓	✓	✓	✗

 May either increase or decrease  Increasing effect  Decreasing effect  Does not affect

After parametric analyzes, fine tuning is done to obtain desired bandwidth for both lower and upper bands. The desired resonance frequency is about 1227 MHz and 20 MHz bandwidth for lower band. On the other hand, it is desired to obtain the resonance frequency 1590 MHz for the upper band and 50 MHz bandwidth. The desired bandwidth is achieved for the values listed in Table 3.3. Figure 3.24 shows the return loss after the fine tuning.

Table 3.3 Values of the parameters after tuning

Name of the Parameter	Value of the Parameter (After fine tuning)
R_outerAr	29mm
R_innerAr	22mm
R_cp	23.8mm
H1	9mm
H2	1mm
L_feed	11.5mm

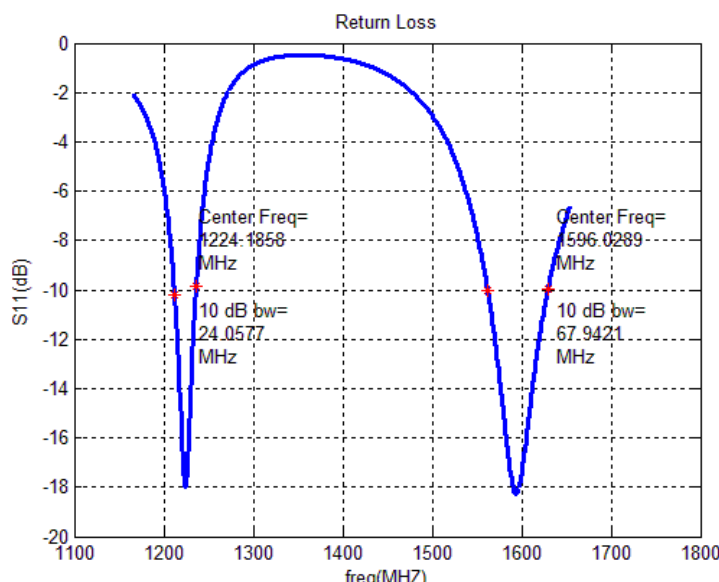


Figure 3.24 Return loss of the antenna after fine tuning

As can be seen from Figure 3.24, desired bandwidth for each resonance is achieved. Directivity of the simulated antenna is shown in Figure 3.25 and 3.26 for each resonance.

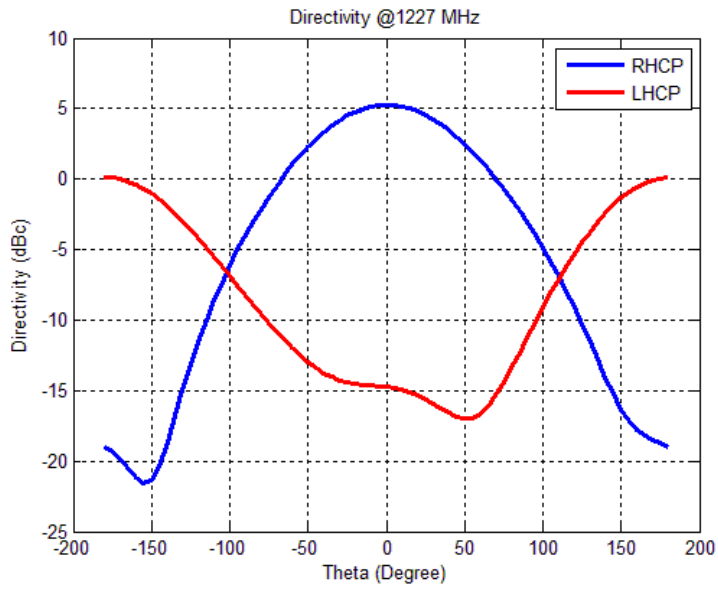


Figure 3.25 RHCP directivity of the antenna at 1227 MHz

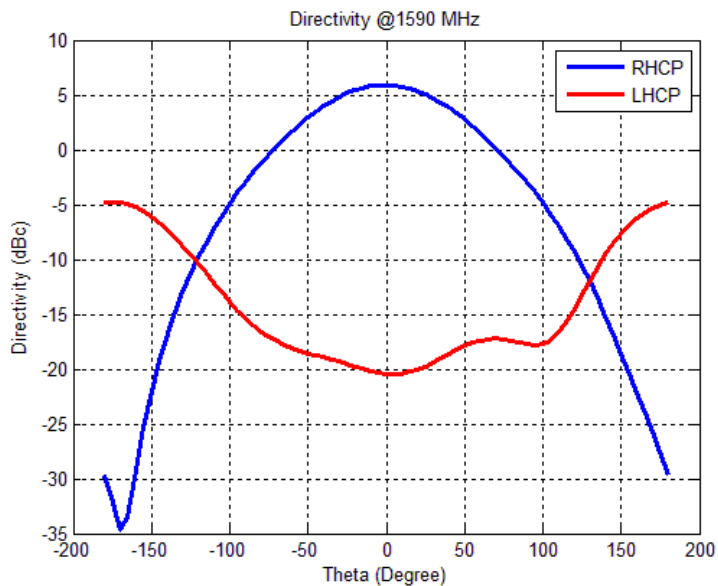


Figure 3.26 RHCP directivity of the antenna at 1590 MHz

Up to this stage, the circular polarization of the antenna was provided by providing a phase difference of 90 degrees to the ports fed by the antenna. In Chapter 4, the design of a 90 degree coupler for feeding the two ports is discussed.

CHAPTER 4

ANALYSIS and DESIGN of COUPLER

Couplers and power dividers may be used in feeding structures of an antenna in various ways. Mostly they are used to achieve the desired amplitude and phase requirements of each antenna element in an antenna array. Couplers are also used to obtain circular polarization in antennas. As mentioned in [2], two orthogonal feed with the phase difference of 90 degree provides circular polarization. Couplers may be a three or four port components. “*Three port networks take the form of T junctions or other power dividers, on the other hand four port networks take the form of directional couplers and hybrids*” [2]. Directional couplers may be designed for any power division, but hybrids generally have equal power division. Directional couplers are four port networks where one port is isolated from the input port. General directional coupler symbol is shown in Figure 4.1.

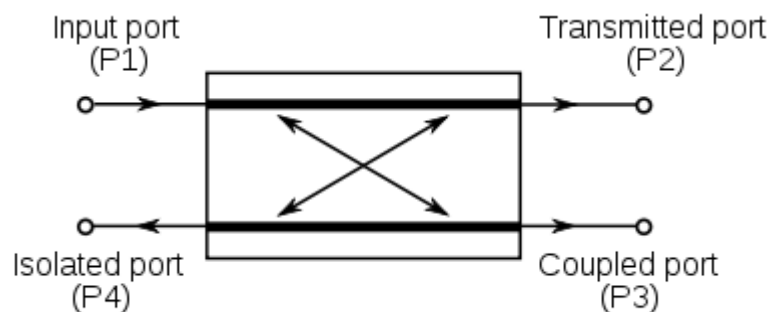


Figure 4.1 General directional coupler symbol

As can be seen in Figure 4.1, there are four ports where one is regarded as the input, one is regarded as transmitted (through), the other one is regarded as the coupled port and the last one is regarded as isolated which is usually terminated by a match load. Common desired features of the couplers are wide bandwidth, good return loss characteristic for all ports when the other ports are matched. General coupler parameters are described below.

- **Coupling Factor**

Coupling factor is the main parameter of a coupler and it is a negative quantity that cannot exceed 0 dB. Coupling factor is defined as in equation (4.1).

$$C = 10 \log\left(\frac{P_3}{P_1}\right) \text{ dB} \quad (4.1)$$

where P1 is the input power from port 1 and P3 is the output power from port 3 in Figure 4.1. In equal power division coupling factor is equal to -3 dB. In practice coupling factor is not higher than -3 dB, because more than -3 dB would result in more power output from coupled port than through port.

- **Loss**

Insertion loss and coupling loss are the main source of the loss. Below equations describe the insertion loss and coupling loss.

$$\text{Insertion loss: } L_i = -10 \log\left(\frac{P_2}{P_1}\right) \quad (4.2)$$

$$\text{Coupling loss: } L_c = -10 \log\left(1 - \frac{P_3}{P_1}\right) \quad (4.3)$$

In a real coupler, there are also losses such as, dielectric loss, conduction loss and mismatch loss.

- **Isolation**

Isolation of a coupler can be specified as the difference of signal levels between the input and isolated ports when the other ports are terminated with a matched load. Isolation can be defined as:

$$I = -10 \log\left(\frac{P_4}{P_1}\right) \quad (4.4)$$

In real couplers it is desired to obtain high isolation between the input and isolated ports.

- **Amplitude Balance**

This parameter is related to difference of the signal levels between the output ports. In hybrid couplers, equal power at the through and coupled port, i.e., 0 dB difference is desired. In practice, however, there is an inevitable difference between the output ports and the designer tries to minimize this difference. This parameter is a frequency dependent parameter.

- **Phase Balance**

Phase difference between the output ports of a hybrid may be 0° , 90° , 180° depending on the desired phase difference. It is important to minimize the deviation of this phase difference from the desired value and its variations over the operating bands.

There are various power dividers proposed in literature. To choose the appropriate one, one should provide the design requirements. Design requirements in this work are listed below;

- 3 dB power division.
- 90 degree phase difference between the output ports.
- About %28 bandwidth (1210-1610 MHz)

Above requirements can be provided by a branchline coupler. In this chapter, analysis and design of the branchline coupler is studied.

4.1 Analysis and Design of a Branchline Coupler

The branchline couplers are the simplest forms to obtain quadrature hybrids that divide the power equally by 90 degree phase difference between the output ports. Branchline couplers are often produced by using microstrip or stripline. Figure 4.2 shows the basic branchline coupler.

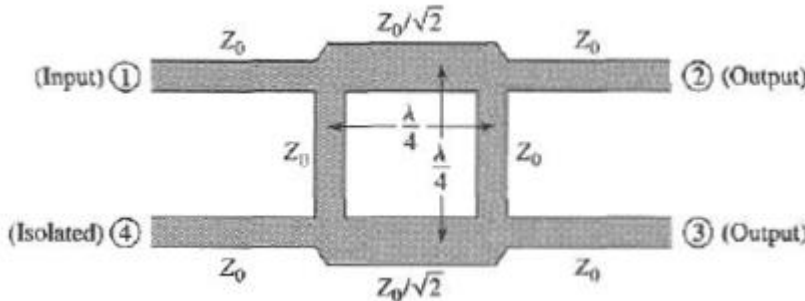


Figure 4.2 Basic branchline coupler [21]

As it can be seen from Figure 4.2, each transmission line is a quarter wave length. A signal applied the input port is divided into two quadrature signals on port 2 and port 3, while input port is isolated from the port 4. It is also possible to use the branchline coupler for unequal power division. The impedance values of opposite arms can be varied. Different impedances allow unequal power divisions. Figure 4.3 shows the unequal power division.

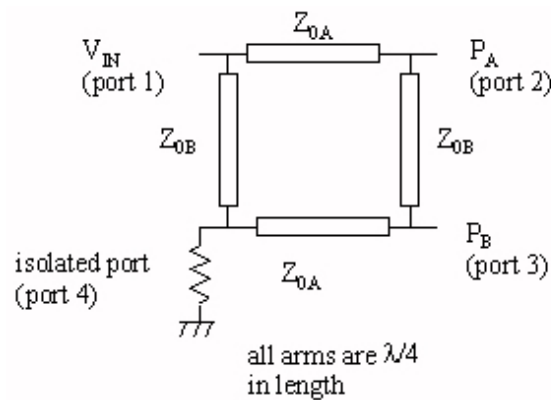


Figure 4.3 Unequal branchline coupler [22]

Even and odd mode analyzes of branchline coupler are given in [21]; The normalized form of the branchline coupler is shown in Figure 4.4.

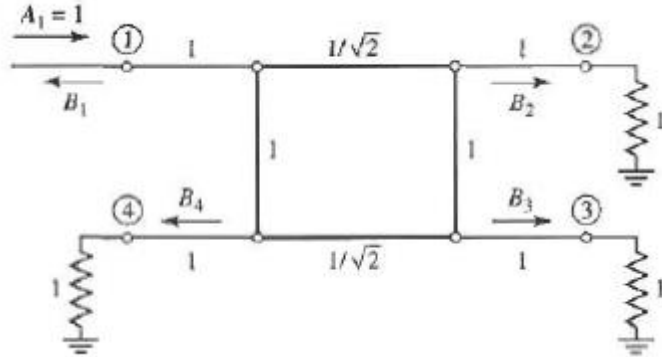


Figure 4.4 Normalized form of the branchline coupler [21]

The circuit of Figure 4.4 can be decomposed into an even mode excitation and odd mode excitation. Figure 4.5 shows the even mode and odd mode excitations. The response of the circuit shown in Figure 4.4 is the sum of the even and odd mode responses.

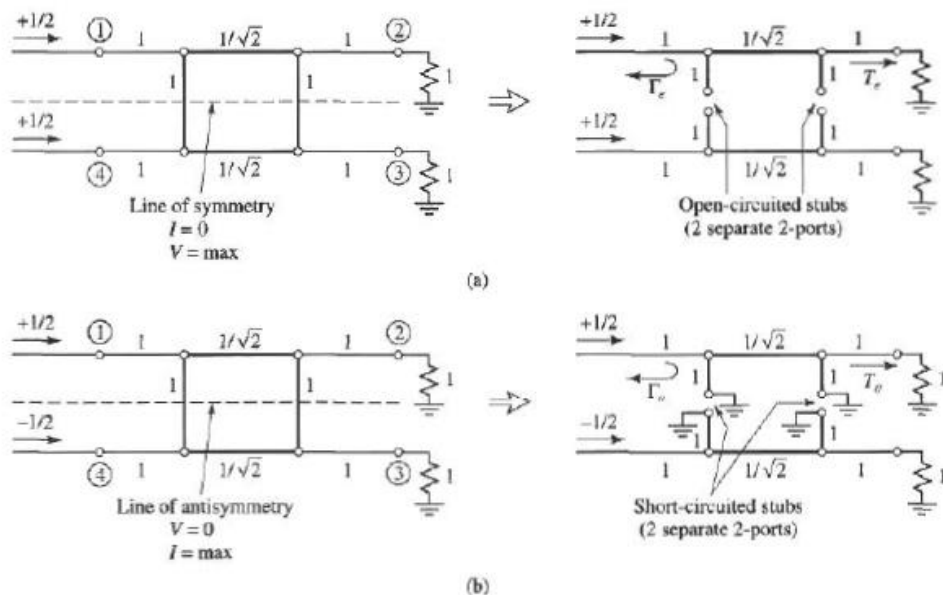


Figure 4.5 (a) even mode excitation, (b) odd mode excitation [21]

Since the amplitudes of the incident waves are $\pm 1/2$ as in Figure 4.5, the amplitudes of the emerging waves at the ports can be defined with below equations.

$$B_1 = \frac{1}{2}(\Gamma_e + \Gamma_o) \quad (4.5a)$$

$$B_2 = \frac{1}{2}(T_e + T_o) \quad (4.5b)$$

$$B_3 = \frac{1}{2}(T_e - T_o) \quad (4.5c)$$

$$B_4 = \frac{1}{2}(\Gamma_e - \Gamma_o) \quad (4.5d)$$

Where $\Gamma_{e,o}$ and $T_{e,o}$ are the even and odd mode reflection and transmission coefficients. First even mode reflection and transmission coefficients are considered. The first step of the calculation is to find ABCD matrices for the circuit. It may be considered that the even mode model is composed of the two $\lambda/8$ open stub and a $\lambda/4$ transmission line. The ABCD parameters of the even mode circuit is given below.

$$\begin{bmatrix} A & B \\ C & D \end{bmatrix} = \begin{bmatrix} 1 & 0 \\ j & 1 \end{bmatrix} \begin{bmatrix} 0 & j/\sqrt{2} \\ j\sqrt{2} & 0 \end{bmatrix} \begin{bmatrix} 1 & 0 \\ j & 1 \end{bmatrix} = \frac{1}{\sqrt{2}} \begin{bmatrix} -1 & j \\ j & -1 \end{bmatrix} \quad (4.6)$$

The ABCD matrices for the even and odd modes can be found by multiplying the ABCD parameters of the each circuit element. The conversion of the ABCD parameters to S parameters is given below, [21]:

$$\Gamma_e = \frac{A+B-C-D}{A+B+C+D} = \frac{-1+j-j+1}{\sqrt{2}} \frac{\sqrt{2}}{-1+j+j-1} = 0 \quad (4.7a)$$

$$T_e = \frac{2}{A+B+C+D} = \frac{2}{\frac{1}{\sqrt{2}}(-1+j+j-1)} = -\frac{1}{\sqrt{2}}(1+j) \quad (4.7b)$$

Similarly for the odd mode;

$$\begin{bmatrix} A & B \\ C & D \end{bmatrix} = \begin{bmatrix} 1 & 0 \\ -j & 1 \end{bmatrix} \begin{bmatrix} 0 & j/\sqrt{2} \\ j\sqrt{2} & 0 \end{bmatrix} \begin{bmatrix} 1 & 0 \\ -j & 1 \end{bmatrix} = \frac{1}{\sqrt{2}} \begin{bmatrix} 1 & j \\ j & 1 \end{bmatrix} \quad (4.8)$$

$$\Gamma_o = \frac{A+B-C-D}{A+B+C+D} = \frac{1+j-j-1}{\sqrt{2}} \frac{\sqrt{2}}{1+j+j+1} = 0 \quad (4.9a)$$

$$T_o = \frac{2}{A+B+C+D} = \frac{2\sqrt{2}}{(1+j+j+1)} = \frac{1}{\sqrt{2}}(1-j) \quad (4.9b)$$

Using (4-7) and (4-9) in (4-5) the appearing waves at the each ports are given the below table 4.1.

Table 4.1 Power values at the coupler ports

	Meaning
B1=0	Port 1 is matched
B2=- $\frac{j}{\sqrt{2}}$	Half power, phase difference between port 1 and port 2 is -90 degree
B3=- $\frac{1}{\sqrt{2}}$	Half power, phase difference between port 1 and port 3 is -180 degree
B4=0	No power to port 4

The desired frequency band for the coupler is between 1200 MHz and 1610 MHz in this thesis. Firstly, substrate should be chosen for the coupler. Since it is desired that the dimensions are small, the thickness of the substrate is chosen to be 0.8mm. The characteristic impedance of the quarter wavelength transmission line;

$$Z = \frac{Z_0}{\sqrt{2}} = \frac{50}{\sqrt{2}} = 35.4 \text{ ohm} \quad (4.10)$$

Stripline geometry is preferred for the coupler instead of microstrip line geometry due to easier mounting to different platforms. The second step of the design is to determine the width of the transmission lines for the 35.4 ohm and 50 ohm. The following setup is prepared in HFSS to determining the width.

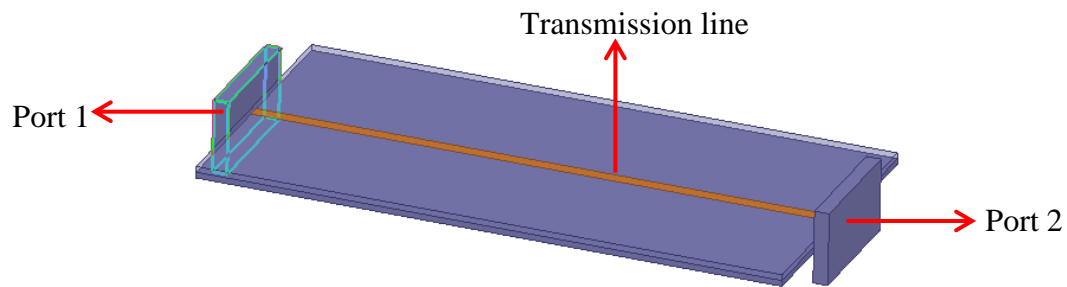


Figure 4.6 Determining the thicknesses of the transmission lines in HFSS

Upper and lower substrates are chosen Rogers 4003 with 0.8mm thicknesses for stripline coupler. Several simulations are done to determine line widths. The line widths are obtained to be 1 mm and 1.8 mm for 50 ohm and 35.4 ohm. For the center frequency the wavelength is calculated and the quarter wavelength is determined. With the obtained values, following coupler is designed.

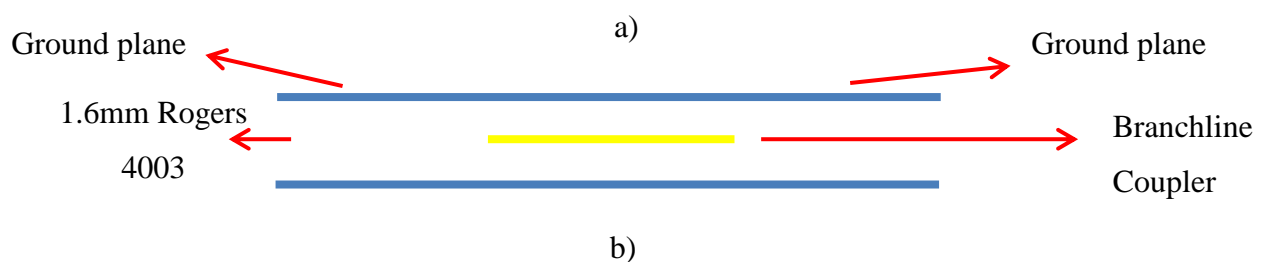
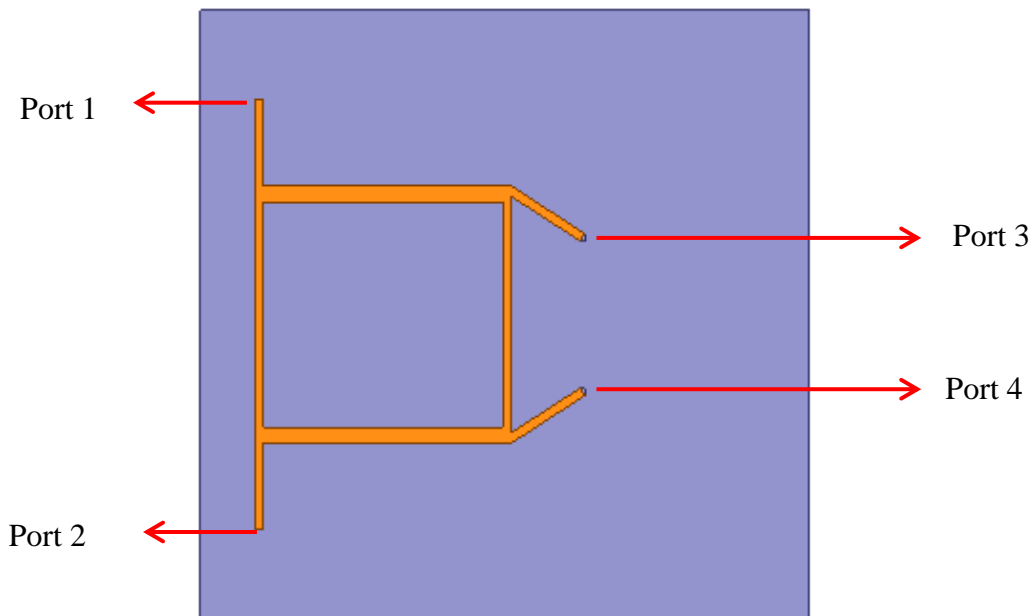


Figure 4.7 Stripline coupler geometry (a) top view, (b) side view

S parameter graphs are given in Figure 4.8. The desired return loss is below -10 dB between 1200 MHz and 1610 MHz and power is divided equally to through and coupled port. Due to the symmetrical structure of the coupler, any port of the coupler can be used as an input port.

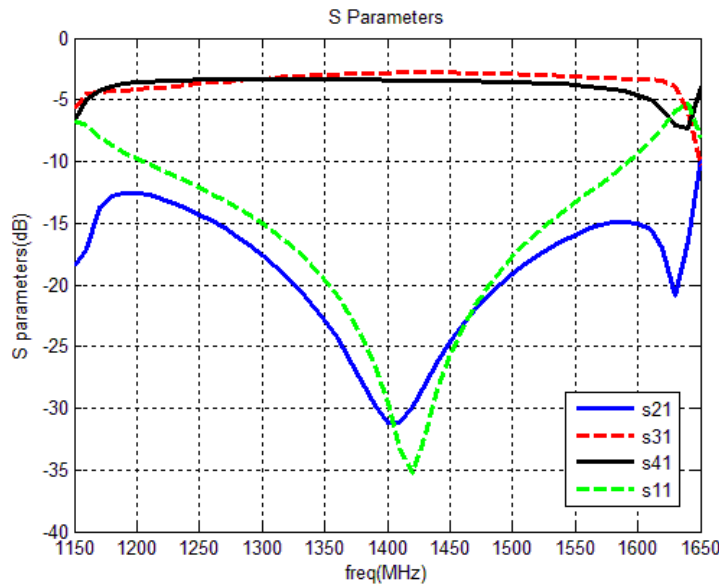


Figure 4.8 S parameters of the stripline coupler

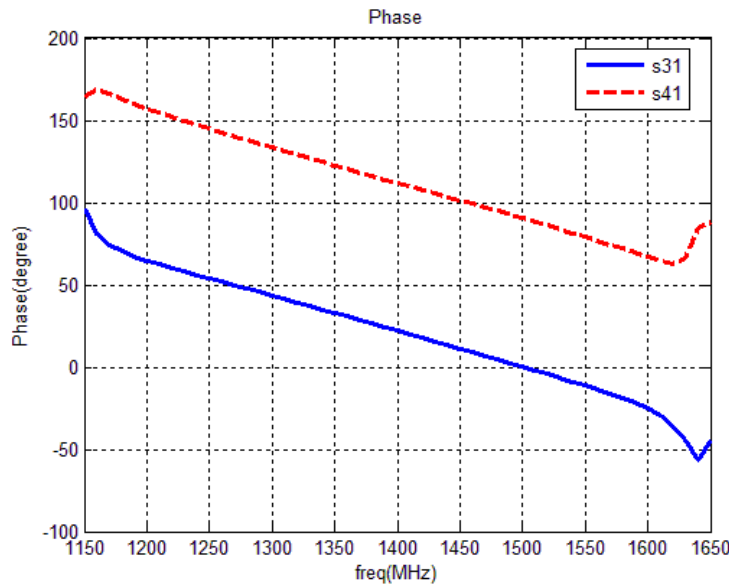


Figure 4.9 Phase of the through and coupled ports

As can be seen from Figure 4.8 there are two extra minima in S₂₁, and also it can be seen from Figure 4.9 that the phase of the S₃₁ and S₄₁ are not linear at the beginning and at the end of the frequency band. The current distribution of the upper ground plane is shown in Figure 4.10. As can be seen from the Figure 4.10 the currents spread over the entire ground plane, this situation leads to higher order

modes being excited. Since the potentials of the two ground planes of the stripline coupler are different, amplitude and phase distribution in stripline geometry may be distorted.

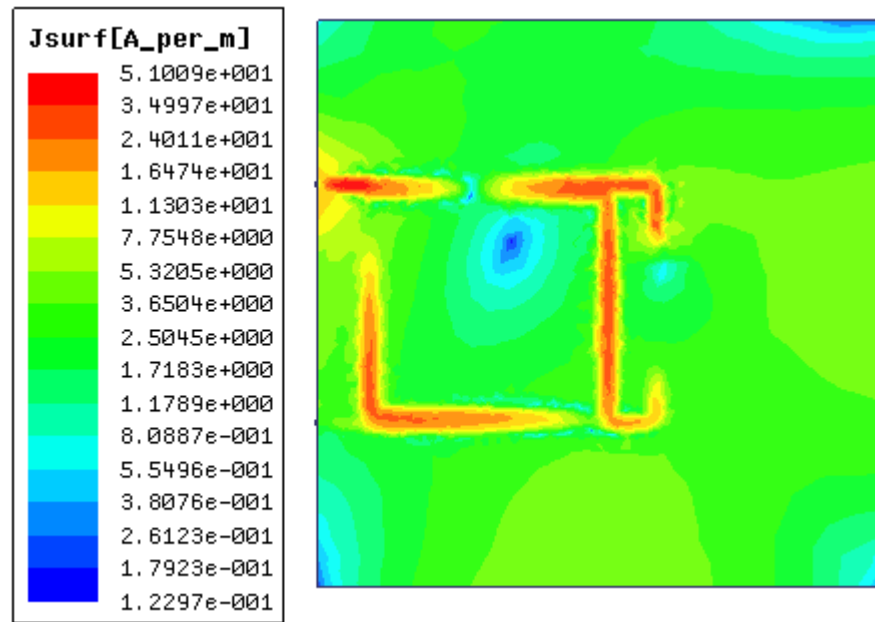


Figure 4.10 Current distribution on the upper ground plane

“Since stripline has two conductors and a homogeneous dielectric, it can support a TEM wave, and this is the usual mode of operation. Like the parallel plate guide and coaxial lines, however, the stripline can also support higher order TM and TE modes, but these are usually avoided in practice (such modes can be suppressed with shorting screws between the ground plane”[21]. As stated in [21], second step of the design is shorting the ground planes from some points. Coupler with shorting pins is shown in Figure 4.11.

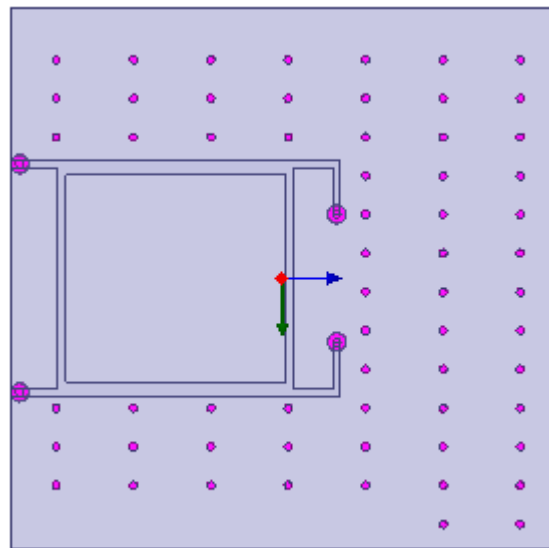


Figure 4.11 Coupler with shorting pins

The shorting pins prevent the excitation of the higher order modes. Current distribution of the upper ground plane in this case is shown in Figure 4.12. With shorting pins currents are damped on the ground planes, so higher order modes are prevented.

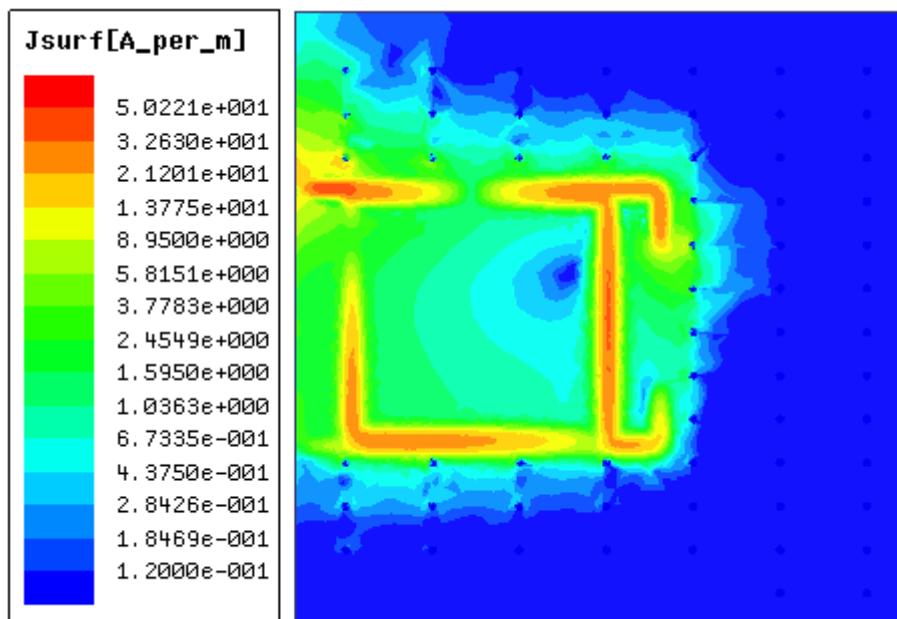


Figure 4.12 Current distribution on the upper ground plane

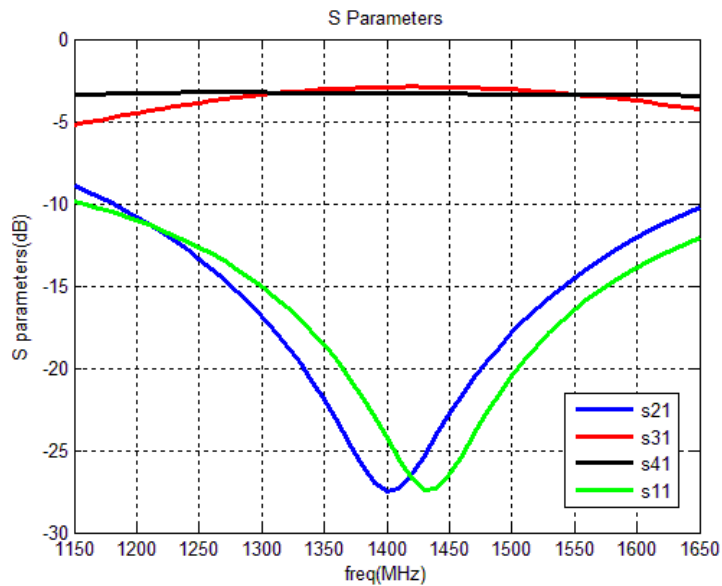


Figure 4.13 S parameters of the coupler with shorting pins

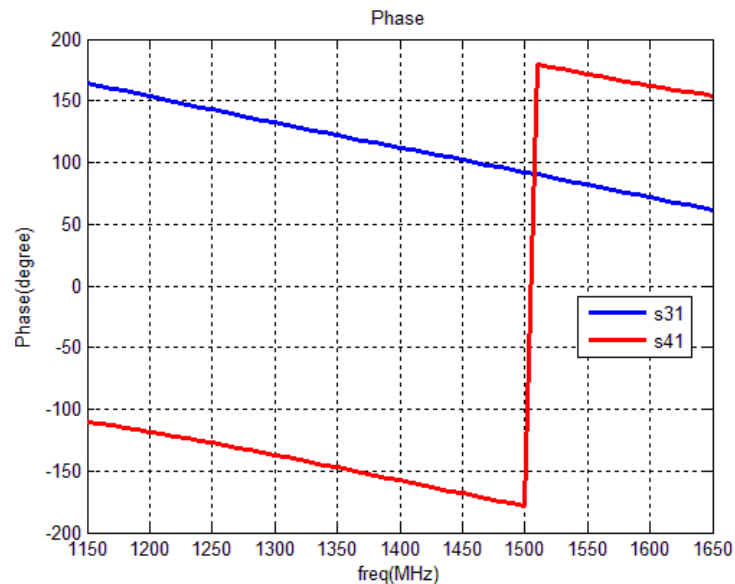


Figure 4.14 Phase of the through and coupled ports

Figure 4.13 and Figure 4.14 shows that, shorting pins fix the problems due to excitation of higher order modes. Amplitudes of the through and coupled ports are very similar. Also Figure 4.14 shows the 90 degree phase difference between the output ports.

CHAPTER 5

AMPLIFYING CIRCUIT DESIGN

5.1 Introduction

GPS signals are extremely weak since they arrive from a long distance. Bad receiving conditions may cause the system to lose the positioning [23]. Active GPS antennas are used to solve this problem. Active antennas have an integrated low noise amplifier (LNA). Using LNA is beneficial for two reasons. The most important advantage is that using LNA prevents overall noise figure of the system to increase due to cable losses 0. The loss of the cable between the antenna and receiver increases the overall noise figure of the system. Integrated LNA in the antenna helps to reduce the overall noise figure of the system and results in better sensitivity. Generally active antennas are preferred if the RF cable length between the receiver and antenna is long.

Noise floor limits the smallest signal that can be detected by the receiver 0. If the noise floor of the receiver is high, the weak signals from the GPS satellites may not be detected. In order to reduce the noise figure and thereby improve the sensitivity, LNA is used in the front end. In this section, active circuits of the GPS antennas are investigated.

There are two main topologies in the literature for GPS antennas. The first one consists of a filter and a LNA. The topology is shown in Figure 5.1.

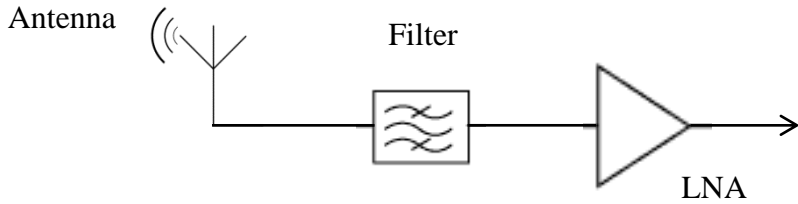


Figure 5.1 GPS antenna system with RF filter and LNA

The antenna system shown in Figure 5.1 is connected to the receiver with an RF cable. For the second topology, the received signal from the antenna is applied to a LNA first and then passes through a RF filter and a second LNA. Figure 5.2 shows the block diagram of the second topology.

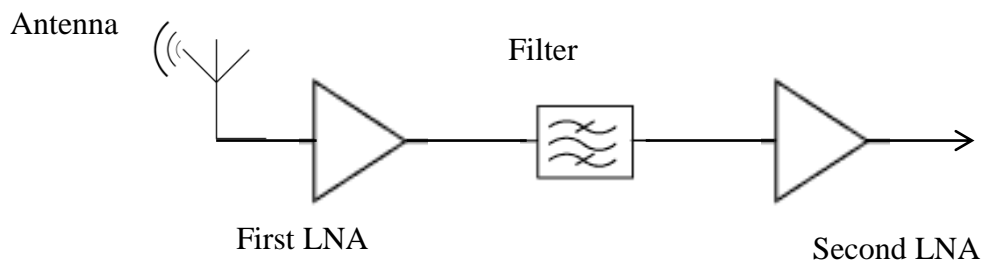


Figure 5.2 GPS antenna system with LNA, RF filter and LNA

Both systems have some advantages and disadvantages. It is necessary to have a close look at the parameters noise and selectivity. As the GPS signals are weak, high sensitivity is an important parameter for the receivers. This can be achieved by proper design of the front end circuit. Noise figure of the first topology is given below [23].

$$F_G = F_{\text{Filter}} + (F_{\text{LNA}} - 1) / G_{\text{Filter}} \quad (5.1)$$

where,

- F_G is the overall noise figure,
- F_{Filter} is the noise figure of the filter,
- F_{LNA} is the noise figure of the LNA,
- G_{Filter} is the gain of the filter (insertion loss of the filter)

Noise figure of the second topology is given in (5.2) [23].

$$F_G = F_{LNA1} + (F_{Filter} - 1)/G_{LNA1} + (F_{LNA2} - 1)/(G_{LNA1} G_{Filter}) \quad (5.2)$$

Where,

- F_{LNA1} is the noise figure of the first LNA,
- G_{LNA1} is the gain of the first LNA,
- F_{LNA2} is the noise figure of second LNA

In the first topology, the insertion loss of the filter must be small since it directly affects the overall noise figure. Both the first term and second term in (5.1) will be large if the insertion loss of the filter is high. Therefore, choosing a filter with very low insertion loss is very critical for this topology.

On the other hand, if the gain of the first LNA, G_{LNA1} , is sufficiently high, the second and third terms in (5.2) become negligible, and the noise figure of the second topology is significantly determined by the first LNA. There are also disadvantages of the second topology. Since the LNA is in the first stage of the circuit, strong interfering signals may drive the LNA into saturation. Due to the high input power, the LNA goes into compression and the gain is reduced. The sensitivity of the system is reduced. P1 dB point is an important parameter for the LNA. The P1 dB point is reached when the input power is so high that the gain of the LNA is reduced by 1 dB. After this point, if the input power is increased further, the gain of the amplifier decreases even more, and eventually the LNA may be damaged. Table 5.1 summarizes the two topologies.

Table 5.1 Comparison of the two topologies

	Filter +LNA	LNA +Filter +LNA
Noise Figure	High	Medium
Gain	High	High
Sensitivity	Medium	High
Price	Medium	High
Design Effort	Medium	High

5.2 Amplifying Circuit Design for GPS

In this section the design of the amplification circuit for dual band antenna is studied. Due to the lower cost, and simpler design the first topology mentioned in section 5.1 is preferred. Since the antenna is dual band, a dual band filter is necessary. In order to reduce the noise figure low insertion loss filters are required. The first filter should pass the GPS L2 band (1227.6 MHz), while the second filter passes the GPS L1 (1575.42) and GLONASS L1 (1605 MHz) signals. Filters with AFS14A34-1588.66-T3 [28] and AFS20A20-1227.60-T3 [27] manufacture type numbers from ABRACON Corporation [26] are chosen due to their low insertion loss.

Since the antenna is fed from a single connector, these two filters must be placed on the same transmission line. T-junction can be used to combine two band pass filters. However, the input impedance of the filters should be investigated, firstly. Since the impedance seen at the input will be obtained by paralleling the input impedances of the filters, the input impedances of the filters will directly affect the return loss at the input. So when the filters are combined with a T junction, something must be done to improve the return loss at the input. There are two ways to improve the return loss and transfer maximum energy to the filters. The first way is to tune the arm lengths and arm widths of the T junction to achieve desired return loss at the input. The tuning process of the lengths and widths of the arms is

done in AWR Microwave Office ® commercial software. Figure 5.3 shows the simulation model of the T junction.

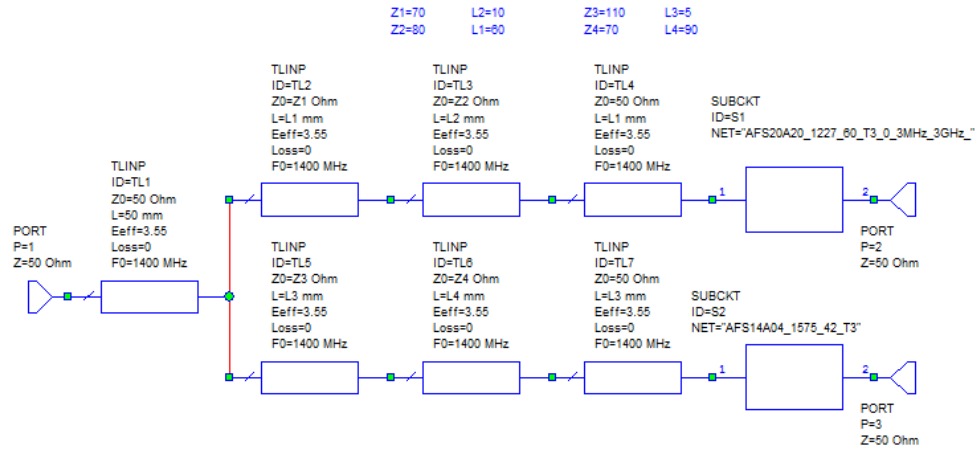


Figure 5.3 T junction simulation model

The arm length and widths of the T junction are optimized in AWR. Figure 5.4 shows the S parameters of the T junction with the optimized values of arm lengths and arm widths.

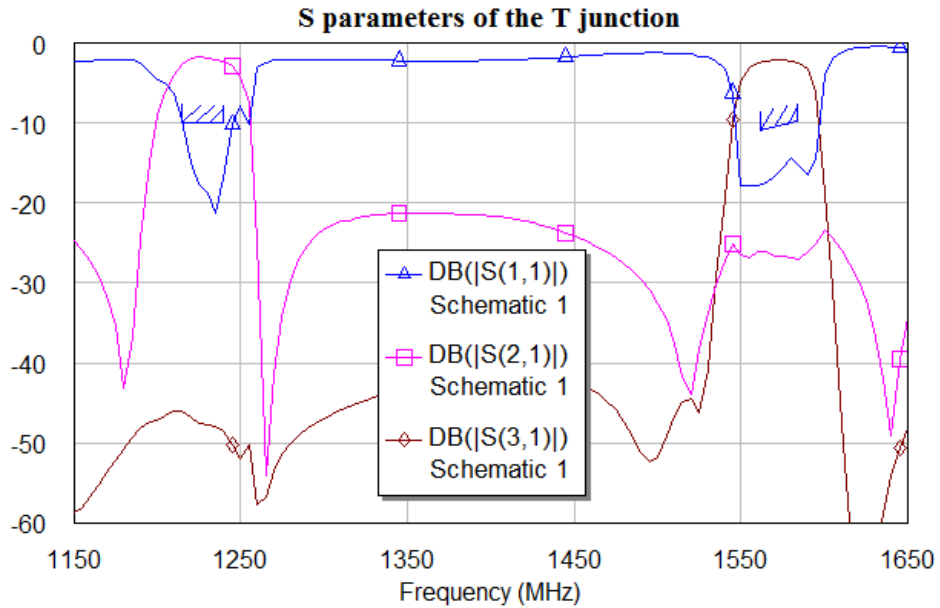


Figure 5.4 S parameters of the T junction

As can be seen from Figure 5.4 the return loss of the T junction is below -10 dB over the desired bands. This means that the effects of the return loss on the overall loss will be smaller with the optimized values of arm lengths and widths.

The second way to improve the return loss at the input is to use a diplexer. Diplexer is a three port network that splits the signal from a common port into other two ports dependent on frequency 0. Generally diplexers consist of a low pass filter and a high pass filter. For our application, diplexer configuration is shown in Figure 5.5.

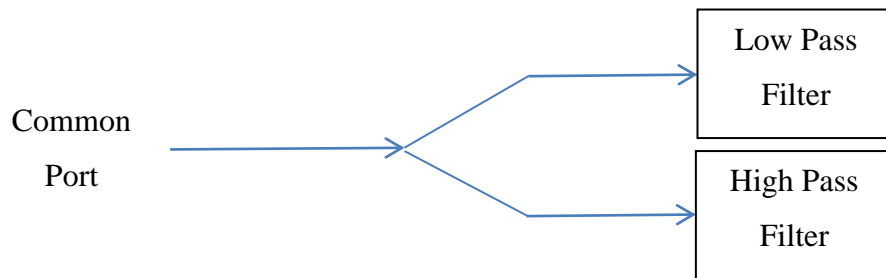


Figure 5.5 Configuration of the diplexer

Return loss parameter of the diplexer should be good at the desired frequencies to transfer maximum power. Cut off frequencies of the filters are adjusted to a frequency that is between the two desired bands. In our application, 1400 MHz is chosen for the cut off frequencies of the filters. Insertion loss of the low pass path of the diplexer must be good at below 1400 MHz. On the other hand, insertion loss of the high pass path of the diplexer must be good at above 1400 MHz. To combine the band pass filters, diplexer configuration is used in this thesis.

5.2.1 Design of the Diplexer

As mentioned before, diplexer consists of a low pass filter and a high pass filter. Firstly, low pass filter is designed. Equally ripple low pass filter prototype [30] is chosen for the low pass filter. All simulations are done in AWR Microwave Office ® commercial software. As shown in Figure 5.6, prototype structure with a series first element is chosen.

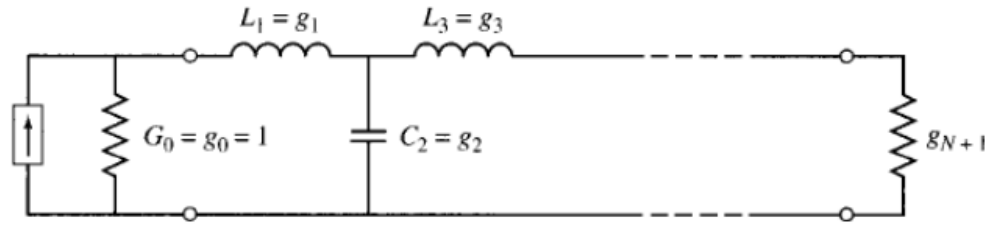


Figure 5.6 Prototype beginning a series element 0

Cut off frequency is chosen to be 1400 MHz and it is aimed to obtain about 15 dB attenuation at 1650 MHz. Thus we have,

$$\omega = 1650 \text{ MHz}$$

$$\omega_c = 1400 \text{ MHz}$$

where ω_c is the cut off frequency and ω is the frequency at which the desired attenuation is attained.

$$\left| \frac{\omega}{\omega_c} - 1 \right| = \frac{1650}{1400} - 1 = 0.1786 \quad (5.3)$$

As can be seen from Figure 5.7 order of the filter must be greater than 6 to achieve 15 dB attenuation at the desired frequency.

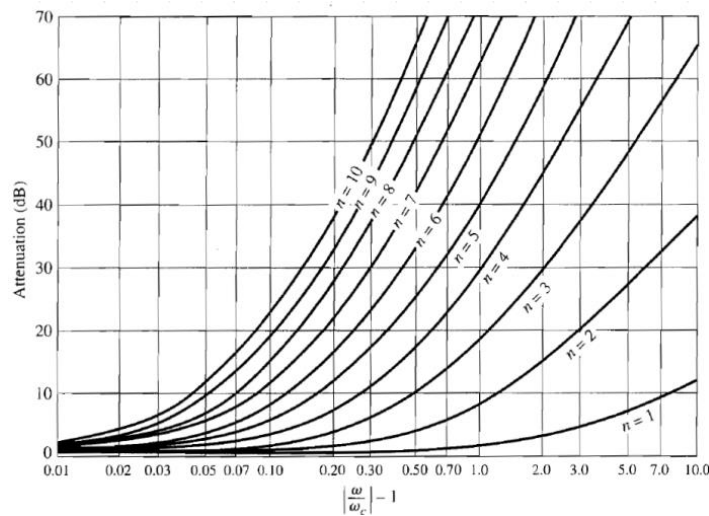


Figure 5.7 Attenuation versus normalized frequency for equal ripple filters [30]

Table 5.2 gives the low pass prototype element values as,

$$g_1 = 1.7254 = L_1$$

$$g_2 = 1.2479 = C_1$$

$$g_3 = 2.6064 = L_2$$

$$g_4 = 1.3137 = C_2$$

$$g_5 = 2.4758 = L_3$$

$$g_6 = 0.8696 = C_3$$

Table 5.2 Element Values for Equal Ripple Low Pass Prototype

N	0.5 dB Ripple										
	g_1	g_2	g_3	g_4	g_5	g_6	g_7	g_8	g_9	g_{10}	g_{11}
1	0.6986	1.0000									
2	1.4029	0.7071	1.9841								
3	1.5963	1.0967	1.5963	1.0000							
4	1.6703	1.1926	2.3661	0.8419	1.9841						
5	1.7058	1.2296	2.5408	1.2296	1.7058	1.0000					
6	1.7254	1.2479	2.6064	1.3137	2.4758	0.8696	1.9841				
7	1.7372	1.2583	2.6381	1.3444	2.6381	1.2583	1.7372	1.0000			
8	1.7451	1.2647	2.6564	1.3590	2.6964	1.3389	2.5093	0.8796	1.9841		
9	1.7504	1.2690	2.6678	1.3673	2.7239	1.3673	2.6678	1.2690	1.7504	1.0000	
10	1.7543	1.2721	2.6754	1.3725	2.7392	1.3806	2.7231	1.3485	2.5239	0.8842	1.9841

Using the equations in 5.4, element values are calculated.

$$L_k' = \frac{R_0 L_k}{w_c} \quad C_k' = \frac{C_k}{R_0 \omega_c} \quad (5.4)$$

$$L_1' = \frac{50 \times 1.7254}{2\pi 1400 \times 10^6} = 9.8074 \text{ nH}$$

$$C_1' = \frac{1.2479}{50 \times 2\pi 1400 \times 10^6} = 2.8373 \text{ pF}$$

$$L_2 = \frac{50 \times 2.6064}{2\pi 1400 \times 10^6} = 14.815 \text{ nH}$$

$$C_2 = \frac{1.3137}{50 \times 2\pi 1400 \times 10^6} = 2.9869 \text{ pF}$$

$$L_3 = \frac{50 \times 2.4758}{2\pi 1400 \times 10^6} = 14.073 \text{ nH}$$

$$C_3 = \frac{0.8696}{50 \times 2\pi 1400 \times 10^6} = 1.9772 \text{ pF}$$

The high pass filter is designed by using the same method. Equal ripple high pass filter prototype 0 is chosen for the high pass filter. Cut off frequency is chosen to be 1400 MHz and it is aimed to obtain about 15 dB attenuation at 1200 MHz. Thus we have,

$$\omega_c = 1400 \text{ MHz},$$

$$\omega = 1200 \text{ MHz},$$

As mentioned in [21], low pass to high pass transformation is applied. The frequency substitution given by,

$$\omega \leftarrow -\frac{\omega_c}{\omega} \quad (5.5) [21]$$

can be used to convert the low pass response to high pass response. Equation (5.5) is applied to series reactances and the shunt susceptances.

$$\left. \begin{aligned} jX_k &= -\frac{j\omega_c}{\omega} L_k = \frac{1}{j\omega C'_k} \\ jB_k &= -\frac{j\omega_c}{\omega} C_k = \frac{1}{j\omega L'_k} \end{aligned} \right\} \quad (5.6) [21]$$

Equation 5.6 shows the series inductor L_k must be replaced with the capacitor C'_k and shunt capacitor C_k must be replaced with the inductor L'_k . New component values of the filter are obtained after impedance scaling given in equation (5.7).

$$\begin{aligned} C_k' &= \frac{1}{R_0 \omega_c L_k} \\ L_k' &= \frac{R_0}{\omega_c C_k} \end{aligned} \quad \left. \begin{array}{l} \\ \end{array} \right\} \quad (5.7) [21]$$

To determine the order of the high pass filter equation (5.8) is used.

$$\left| -\frac{\omega_c}{\omega} \right| - 1 = \frac{1400}{1200} - 1 = 0.1667 \quad (5.8)$$

Again, from Figure 5.7, we must use a filter of order $N > 6$ to achieve the desired 15 dB attenuation at desired frequency. The prototype high pass filter has the same parameters as before and are given as,

$$g_1 = 1.7254 = L'_1$$

$$g_2 = 1.2479 = C'_1$$

$$g_3 = 2.6064 = L'_2$$

$$g_4 = 1.3137 = C'_2$$

$$g_5 = 2.4758 = L'_3$$

$$g_6 = 0.8696 = C'_3$$

Using equations (5.7), element values of the high pass filter are calculated below.

$$C_1 = \frac{1}{50 \times 2\pi 1400 \times 10^6 \times L'_1} = \frac{1}{50 \times 2\pi 1400 \times 10^6 \times 1.7254} = 1.3177 \text{ pF}$$

$$L_1 = \frac{50}{2\pi 1400 \times 10^6 \times C'_1} = \frac{50}{2\pi 1400 \times 10^6 \times 1.2479} = 4.5549 \text{ nH}$$

$$C_2 = \frac{1}{50 \times 2\pi 1400 \times 10^6 \times L'_2} = \frac{1}{50 \times 2\pi 1400 \times 10^6 \times 2.6064} = 0.87233 \text{ pF}$$

$$L_2 = \frac{50}{2\pi 1400 \times 10^6 \times C'_2} = \frac{50}{2\pi 1400 \times 10^6 \times 1.3137} = 4.3268 \text{ nH}$$

$$C_3 = \frac{1}{50 \times 2\pi 1400 \times 10^6 \times L_3} = \frac{1}{50 \times 2\pi 1400 \times 10^6 \times 2.4758} = 0.91835 \text{ pF}$$

$$L_3 = \frac{50}{2\pi 1400 \times 10^6 \times C_3} = \frac{50}{2\pi 1400 \times 10^6 \times 0.8696} = 6.5365 \text{ nH}$$

After calculating the element values of both low pass and high pass filters the following circuit is established in AWR Microwave Office ® commercial software. The diplexer circuit has one input and two outputs. One of the outputs is adjusted to pass GPS L2 band, and the other output is adjusted to pass GPS L1 and GLONASS L1 bands.

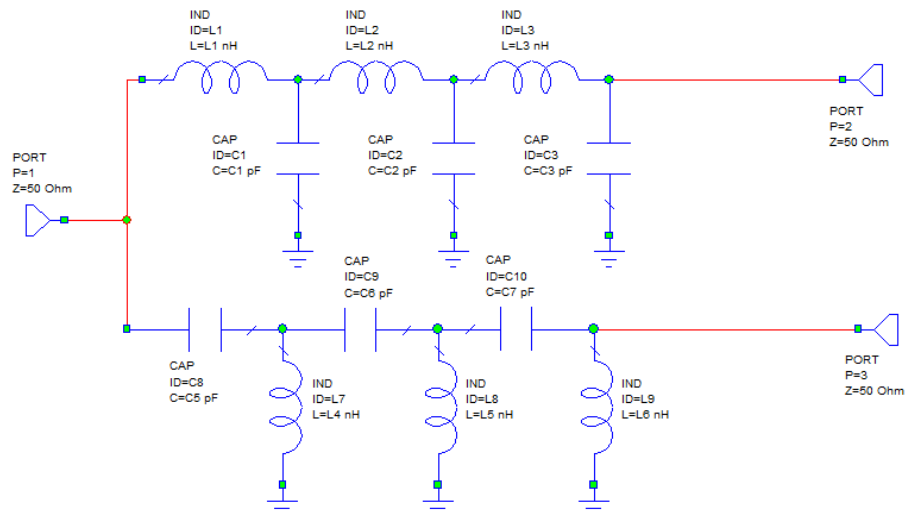


Figure 5.8 Diplexer circuit with lumped elements

Using the optimization tool of the AWR, component values of the diplexer is optimized. The return loss characteristic of the diplexer is tuned on the desired frequency bands. The optimized element values are given in Table 5.3.

Table 5.3 Optimized Element Values

Parameter Name	Parameter Value	Parameter Name	Parameter Value
L_1	7.6 nH	C_1	4.7 pF
L_2	10 nH	C_2	4.7 pF
L_3	8 nH	C_3	3 pF
L_4	3.3 nH	C_4	1.5 pF
L_5	3.3 nH	C_5	1.2 pF
L_6	3.9 nH	C_6	1.6 pF

S parameters of the diplexer with using the optimized element values are shown in Figure 5.9.

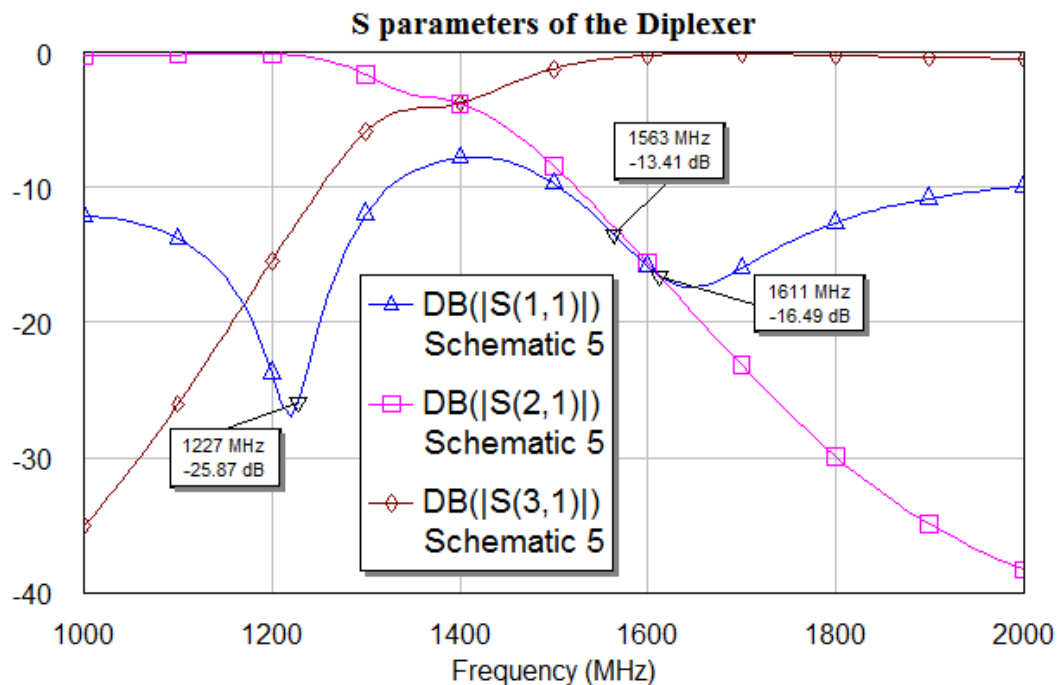


Figure 5.9 S parameters of the Diplexer

As can be seen in Figure 5.9, signal splits into two output port. Matching of the diplexer is good for two desired bands. After designing the diplexer, active circuit is established. The schematic of the active circuit is shown in Figure 5.10.

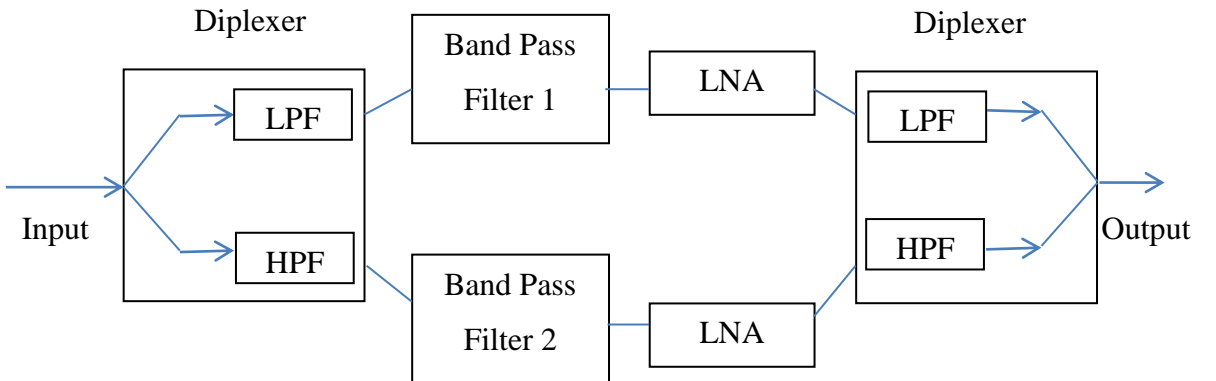


Figure 5.10 Schematic of the active circuit

Band pass filter 1 symbolizes the AFS20A20-1227.60-T3 [27], in addition to this band pass filter 2 symbolizes the AFS14A34-1588.66-T3 [28]. LNA with the part number PMA-545G1+ from Mini-circuits ® [31] is used due to low noise figure characteristic. In addition to low noise characteristic, LNA has about 30 dB gain over the whole desired band. The active circuit that is shown in Figure 5.10 is simulated using the AWR. The insertion loss and return loss of the active circuit is shown in Figure 5.11.

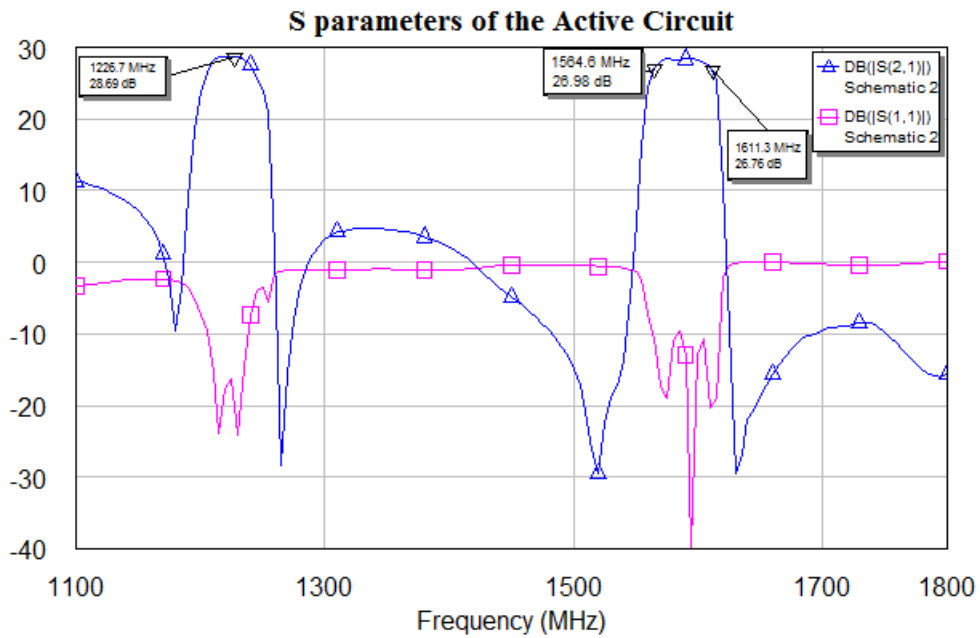


Figure 5.11 S parameters of the Active Circuit

Figure 5.11 shows the gain of the active circuit. The gain of the active circuit at GPS L2 band is about 28 dB, whereas the gain is about 27 dB at the GPS L1 and GLONASS L1 bands. The gain of the LNA is lower at the GPS L1 and GLONASS L1 band than GPS L2 band.

CHAPTER 6

MANUFACTURING ACTIVE DUAL BAND ANNULAR RING COUPLED CIRCULAR PATCH ANTENNA AND MEASUREMENT RESULTS

Up to this chapter, some design examples are investigated. In Chapter 3, the design principles of the annular ring coupled circular patch antenna are given. In Chapter 4, the design principles of the couplers are given. Some prototypes are fabricated by using the optimized design parameters. Active circuit of the antenna is fabricated and all fabricated designs are measured. The measurement results are given in this chapter.

The design which is given in Chapter 3 is produced firstly, in the facilities of ASELSAN A.Ş. using the parameters given in section 3.3.7. Antenna is fabricated by the LPKF Protolaser S milling machine shown in Figure 6.1. The materials used as the dielectric are FR4 and Rogers 5880 as mentioned in Chapter 3. S parameters of the antenna are measured. As can be seen from the Figure 6.2, the dual band operation is achieved, but it is observed that first resonance shifts the higher frequency region. The thickness of the FR4 substrate which we need to produce our antenna is 9 mm. Since this thickness is not a standard thickness for FR4 substrate, 6 pieces of 1.524mm FR4 substrate is used to obtain similar thickness. After FR4 substrates are combined, the Rogers 5880 substrate that has annular ring on it, is combined with the FR4 substrates. The production of the antenna is difficult due to difficulties of combining the substrates. When FR4 substrates are assembled to each other, air can remain between them. This can cause the shift in the resonance frequency.

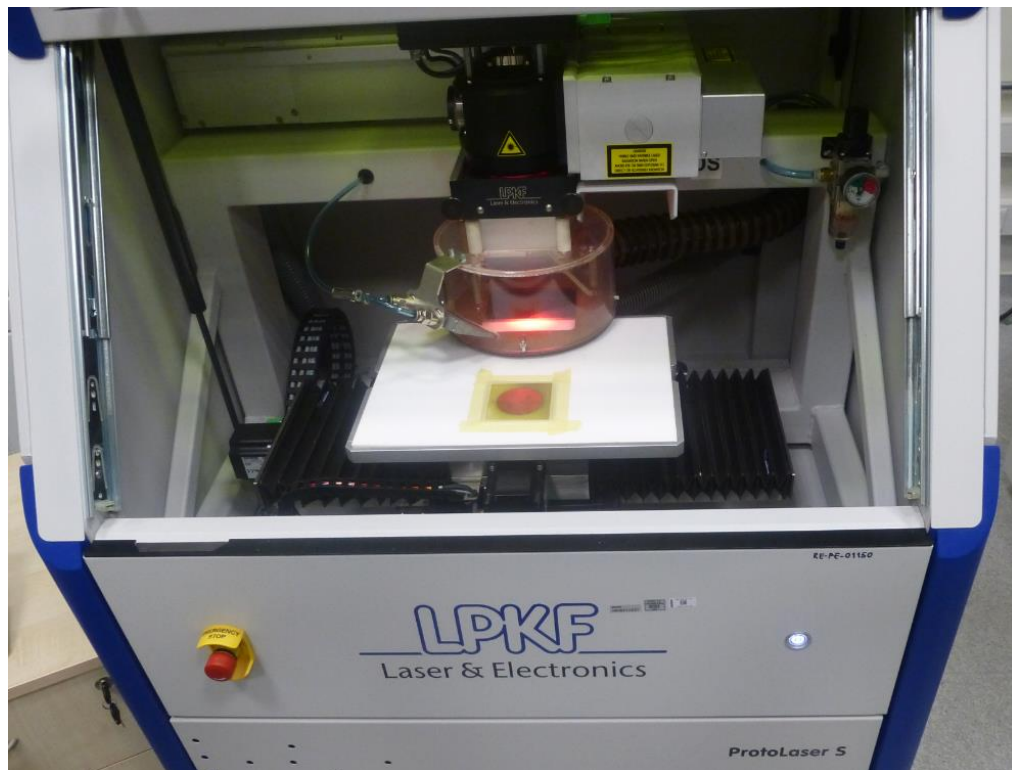


Figure 6.1 Fabrication of the antenna

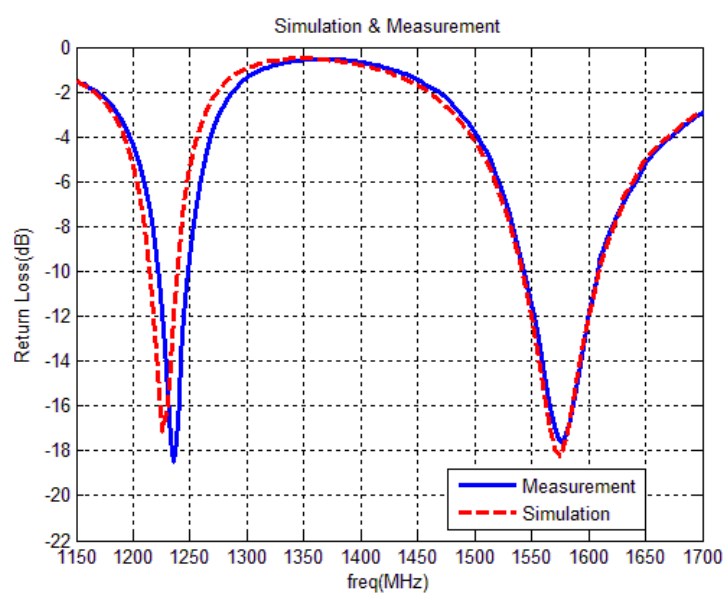


Figure 6.2 Return loss comparison with fabricated and simulated antenna

The produced antenna is shown in Figure 6.3. As can be seen in Figure 6.2, the first resonance is shifted to upper frequency region. This change may be corrected by increasing the outer radius of the annular ring antenna. Some annular ring antennas with different radii are fabricated to optimize the first resonance frequency. Optimized outer radius of the annular ring antenna is 30.5mm. The measured return loss of the antenna with radius 30.5 mm, is shown in Figure 6.4. After the dual band operation is achieved, it is focused on to achieve circular polarization. This time the coupler that is given in Chapter 4 is fabricated. Fabricated coupler is shown in Figure 6.7.



Figure 6.3 Fabricated antenna

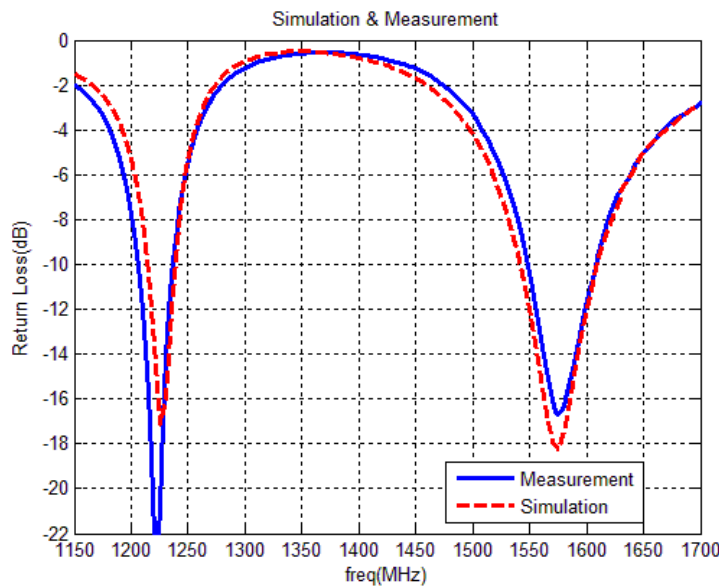


Figure 6.4 Optimized return loss of the antenna

After the fabrication of the stripline coupler is completed, the S parameters of the coupler are measured by network analyzer. The measured parameters of the coupler are shown in Figure 6.5 and Figure 6.6.

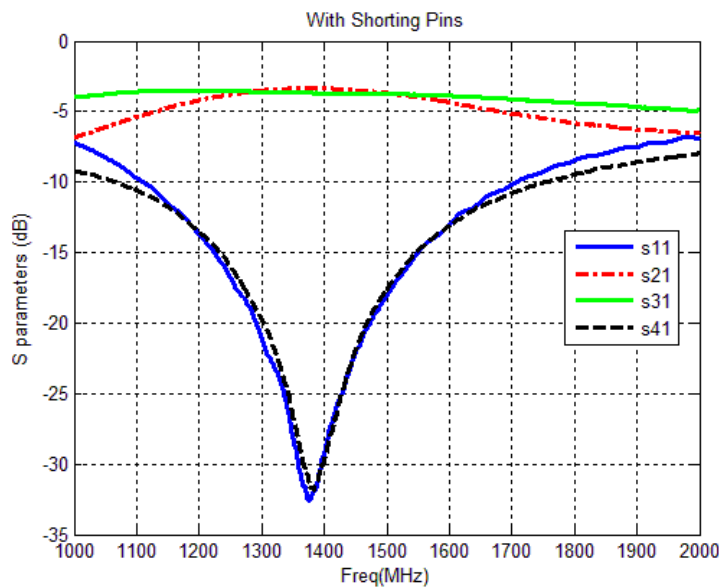


Figure 6.5 S parameters of the stripline coupler

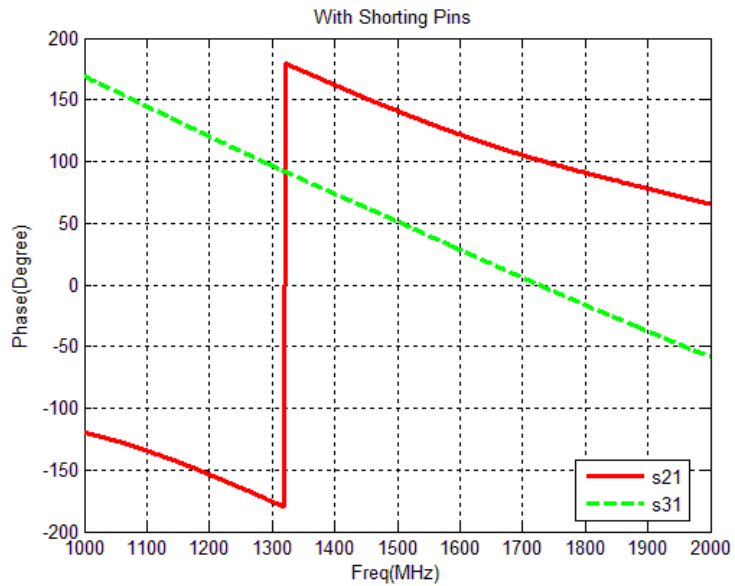


Figure 6.6 Phase of the stripline coupler

As seen in Figure 6.5, the return loss level of the coupler is below -10 dB between the frequencies 1200 MHz and 1610 MHz. Amplitudes of port 2 and port 3 are nearly equal and phase difference between these ports is nearly 90 degree over the desired frequency band. 90 degree phase difference between the port 2 and port 3 provides us circular polarization.

After measurement of the stripline coupler, there is one more step to complete the antenna. The last step is fabrication of the active circuit. As discussed in Chapter 5, the active circuit of the antenna basically comprises of a filter and a LNA. Fabricated active circuit is shown in Figure 6.8. After the fabrication of the active circuit is completed, the S parameters of the active circuit are measured by network analyzer. The circuit needs external 5V DC voltage to feed the amplifiers. The measured S parameters of the active circuit are given in Figure 6.9.

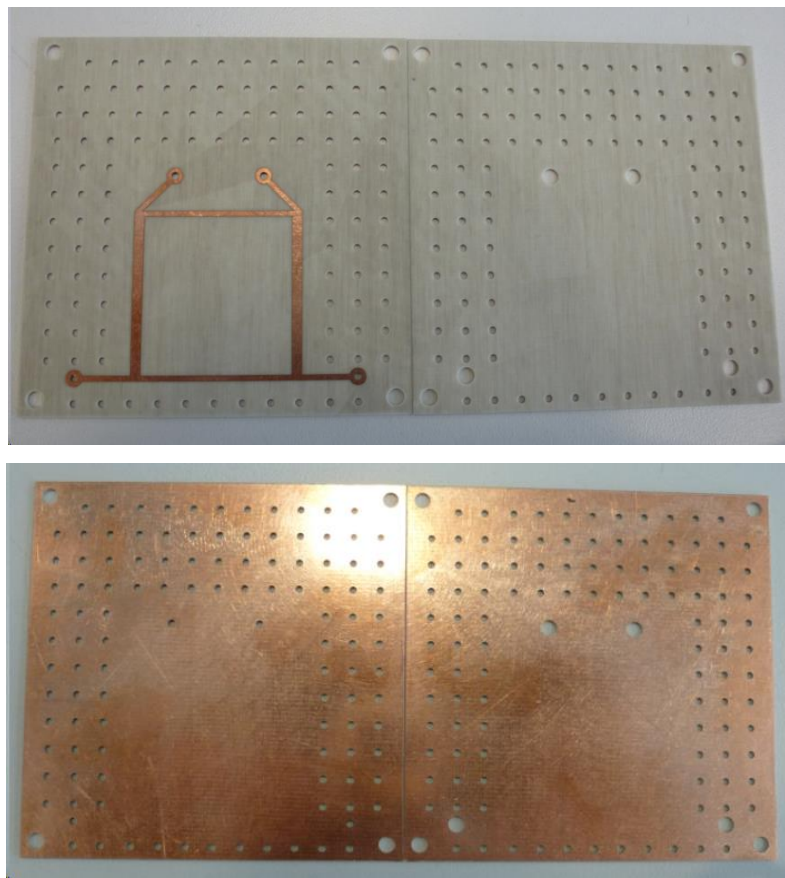


Figure 6.7 Fabricated stripline coupler

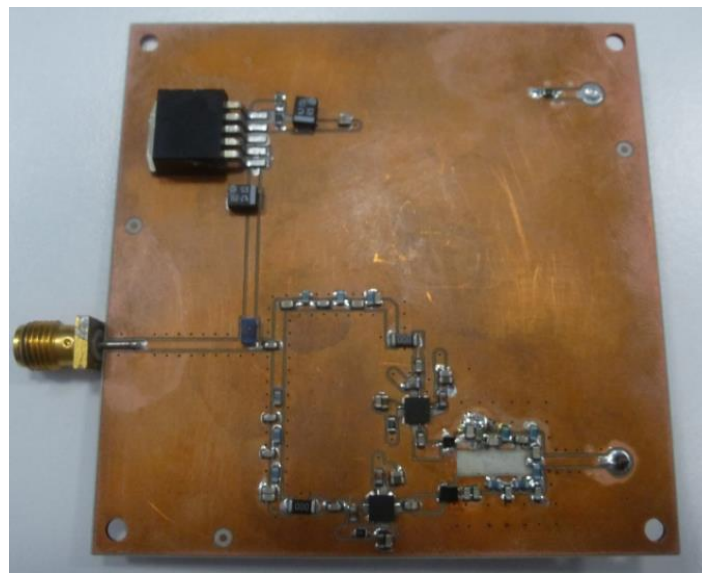


Figure 6.8 Fabricated Active Circuit

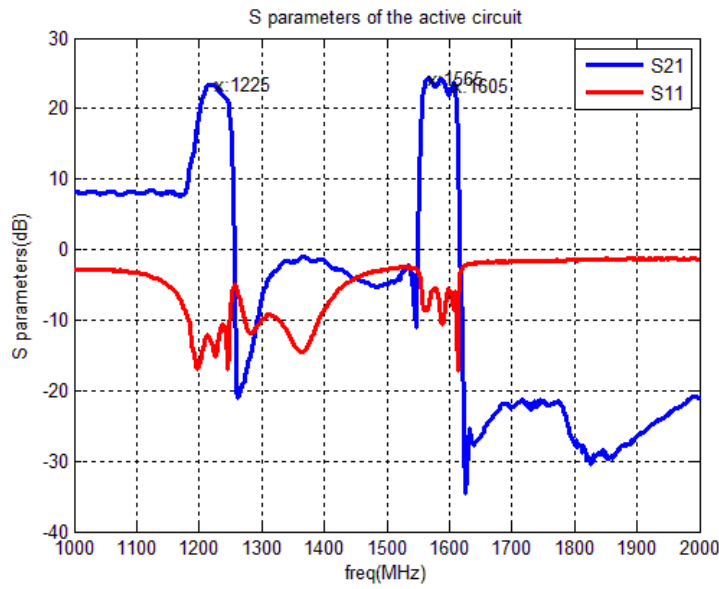


Figure 6.9 S parameters of the active circuit

As can be seen from figure 6.9, the gain of the active circuit is about 24 dB at the desired frequency bands. The reason of the loss of the circuit is diplexer loss. Since lumped components are used in the implementation of the diplexer, the loss of the diplexer is slightly higher than expected. If a diplexer that has high quality factor is used, the loss of the circuit may be less. After s parameter measurements are done, the far field pattern of the antenna is measured. The far field measurements of the antenna are done in SATIMO Starlab Spherical Near Field Measurement System which is shown in Figure 6.10 and 6.11.

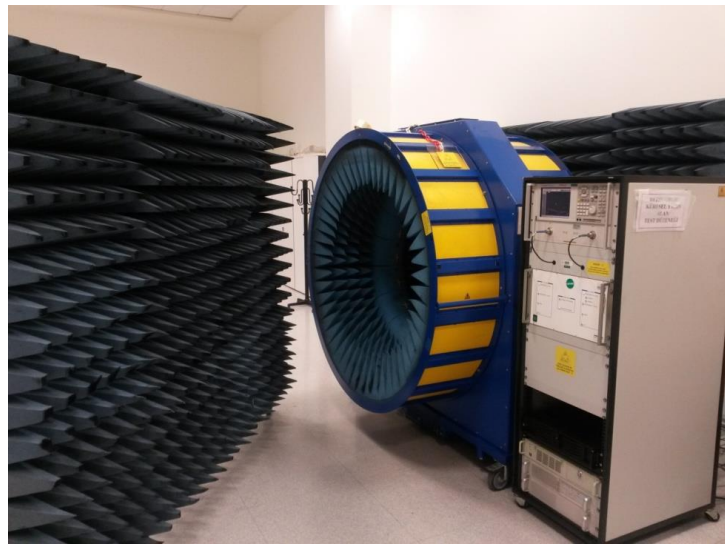


Figure 6.10 SATIMO Near Field Measurement System

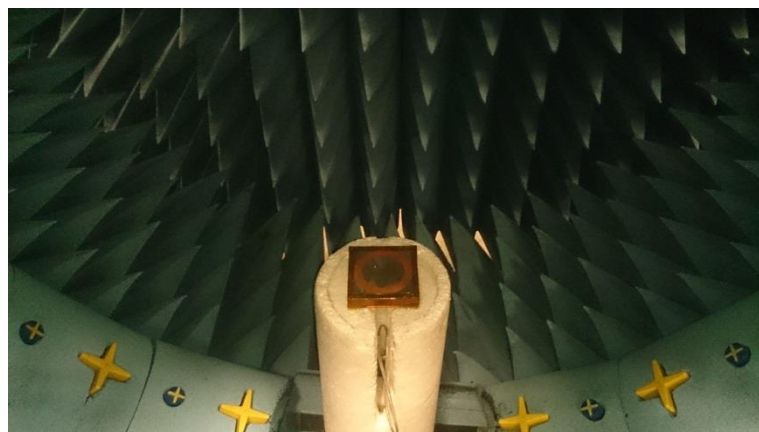


Figure 6.11 Placement of the antenna in SATIMO

Figure 6.12 and Figure 6.13 show the axial ratio comparison of the simulation and measurement results. Both results provide 3 dB axial ratio over the desired band.

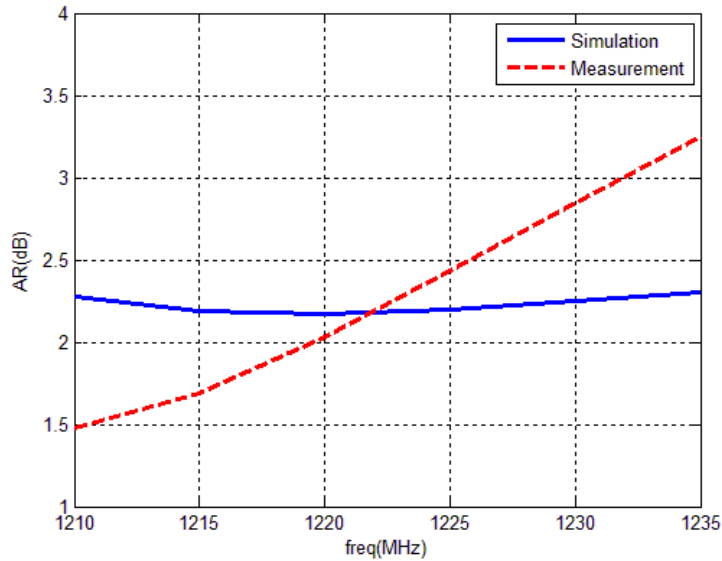


Figure 6.12 Axial ratio of the lower band (GPS L2)

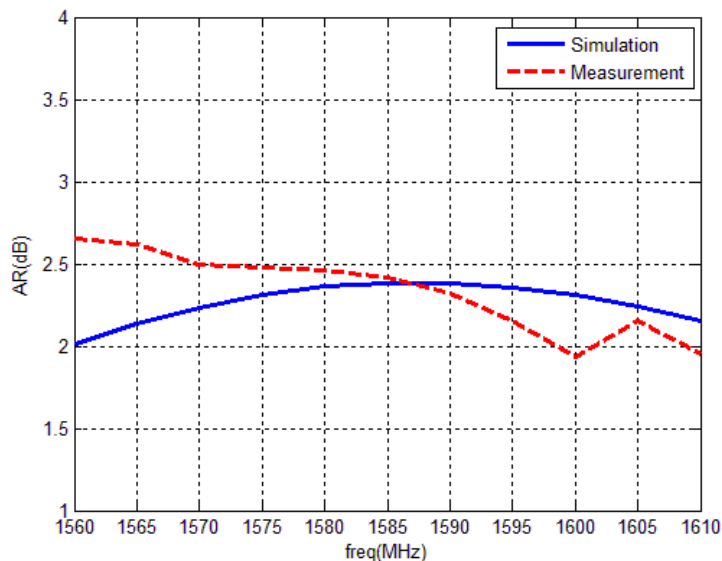


Figure 6.13 Axial ratio of the upper band (GPS L1 and GLONASS L1)

The radiation patterns for RHCP (co-pol) and LHCP (cross-pol) at 1227 MHz, 1575 MHz and 1605 MHz are shown in Figure 6.14, Figure 6.15 and Figure 6.16. The fabricated antenna has nearly 25 dB gain at all desired frequency bands.

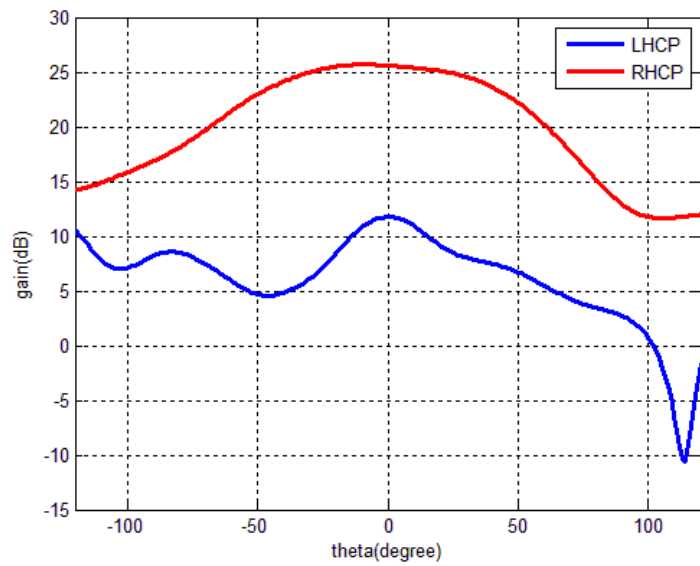


Figure 6.14 Radiation pattern of the antenna at 1227 MHz

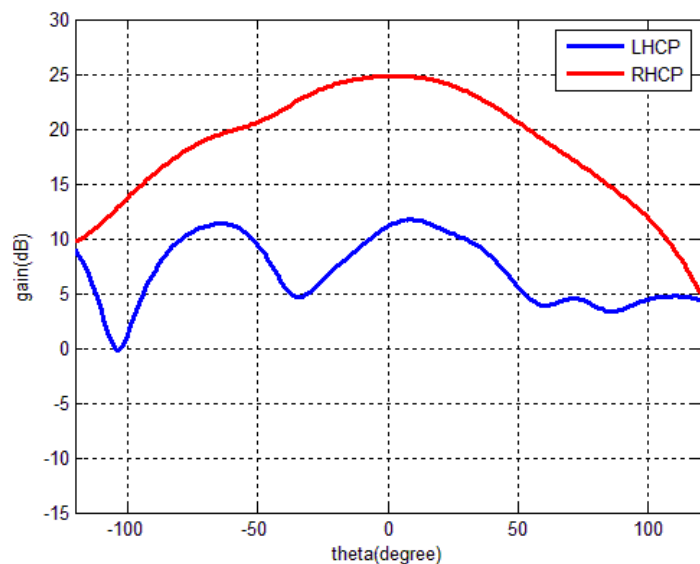


Figure 6.15 Radiation pattern of the antenna at 1575 MHz

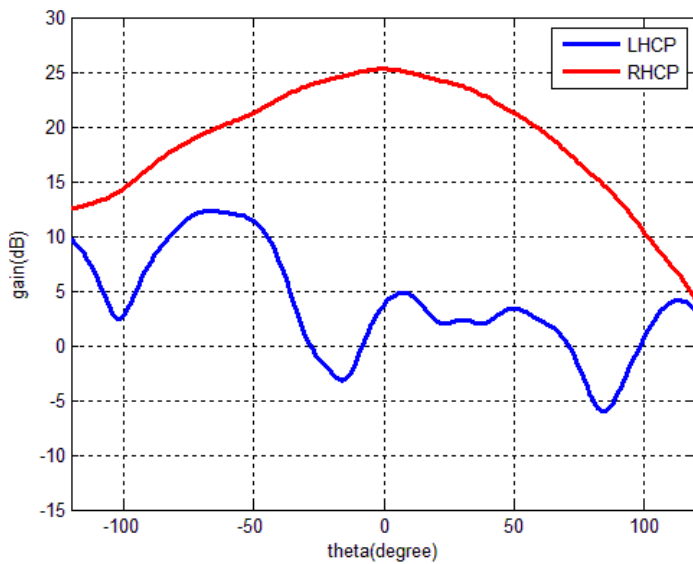


Figure 6.16 Radiation pattern of the antenna at 1605 MHz

The gain of the antenna as a function of the frequency is shown in Figure 6.17. The antenna provides about 25 dB gain at $1227 \text{ MHz} \pm 10 \text{ MHz}$, $1585 \text{ MHz} \pm 20 \text{ MHz}$.

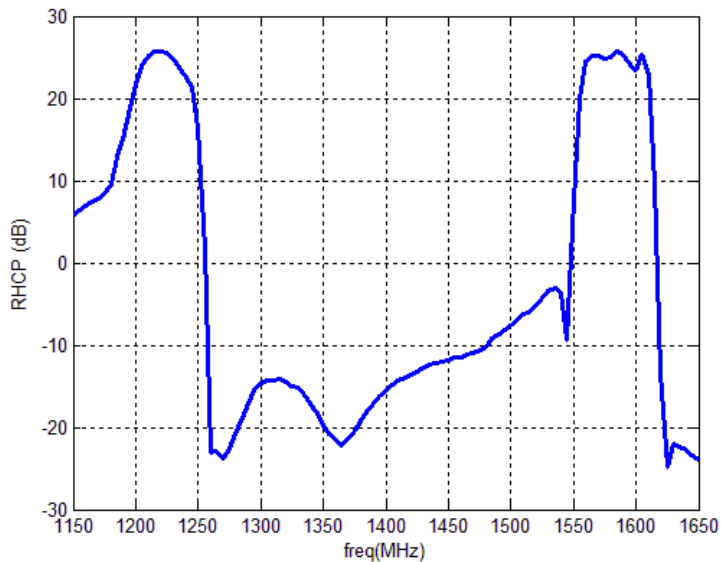


Figure 6.17 Frequency dependent gain of the antenna

CHAPTER 6

CONCLUSIONS

In this thesis, the analysis and design of an active dual band annular ring coupled circular patch antenna is studied. The main motivation is to use this antenna for GPS L1, GPS L2 and GLONASS L1 frequency bands. Dual band operation is achieved by using two antenna elements. Stacked patch configuration is investigated and annular ring antenna and circular patch antenna are stacked. Annular ring antenna is used for GPS L2 band. Circular patch antenna is used for GPS L1 and GLONASS L1 bands. Antenna is designed step by step. Firstly dual feed circular patch antenna is investigated to cover the frequency bands of GPS L1 and GLONASS L1. After that, annular ring patch antenna is stacked with the circular patch antenna to achieve dual band operation. Parametric analyzes are done. The effects on the input impedance and frequency ratio of all antenna parameters are studied. The final design of the antenna is obtained by optimization using HFSS.

Antennas that are used for GPS and GLONASS systems should receive RHCP waves due to GPS and GLONASS satellites radiate RHCP waves. After dual band operation is achieved, it is focused on to achieve circular polarization. Circular polarization techniques are investigated. Suitable method to achieve circular polarization is to use two ports with 90 degree phase shift. For this purpose coupler types are studied. Branchline coupler is preferred since it satisfies the design specs and is easy to design. stripline coupler is designed. During design process, stripline design challenges were encountered. Higher order modes were suppressed by using

shorting pins. The final design of the coupler is obtained by optimization using HFSS.

The last step is to design active circuit of the antenna. GPS signals are very weak and reception may be poor under certain circumstances. Active antennas are used to solve this problem. Some commercial active GPS antennas are investigated. Generally two different topologies are used in commercial applications. The first and basic topology comprises of filter and LNA. The second topology comprises of LNA, filter and again LNA. The advantages and disadvantages of these two topologies are studied. Due to lower cost and simpler design, the first topology is chosen for the active circuit. Filters that have high quality factor and low insertion loss were investigated. Filters from ABRACON Corporation [26] that have manufacture type numbers AFS14A34-1588.66-T3 [28] and AFS20A20-1227.60-T3 [27] are preferred due to their low insertion loss. LNA that has low noise figure is investigated. LNA from Mini-Circuits ® [31] that has manufacture type number PMA-545G1+ is used due to low noise figure characteristic.

After the design of the antenna is completed; antenna, coupler and active circuit is fabricated and measured. Measurement results are compared to the simulation results. The FR4 substrate thickness of the antenna is 9 mm. Since 9 mm substrate thickness is not a standard thickness for the FR4, 6 pieces of FR4 substrate with the thickness of 1.524mm is used. This situation made the production difficult. There can be gaps between the substrates when stacking the substrates. These gaps can affect the resonance frequency of the antenna. As a result, care should be taken not to leave spaces between the substrates while stacking them together. In first prototype the lower resonance frequency is shifted upwards due to manufacturing problems. After production, the radius of the annular ring antenna is optimized to match the resonance frequencies of the manufactured antenna and simulated antenna. After optimization good agreements between simulations and measurements are achieved.

Fabricated stripline coupler is measured and compared with the simulation results. Good agreement is obtained between the simulations and measurements. Active circuit of the antenna is implemented and measured. The gain of the active circuit is measured to be nearly 23 dB. Due to the loss of the diplexer, the gain of the active circuit is lower. Noise figure of the active circuit is higher than expected due to diplexer loss. In order to reduce noise figure, the loss of RF components like filter, between the LNA and antenna should be decreased.

At last, all parts are combined. The antenna is measured in SATIMO Starlab Spherical Near Field Measurement System. The gain of the antenna is measured to be nearly 26 dB for both frequency bands. The axial ratio of the antenna is almost below 3 dB for both frequency bands.

Because of using low dielectric constant substrates, antenna size is larger than commercial GPS antennas. Ceramic substrates are preferred for most commercial GPS antennas. A future study is planned to minimize the antenna size by using high dielectric constant substrates.

REFERENCES

- [1] C.A. Balanis, "Antenna Theory Analysis and Design, Third Edition", John Wiley & Sons, United States of America, 2005.
- [2] R. Garg, P. Bhartia, I. Bahl and A. Ittipoon, "Microstrip Antenna Design Handbook", Artech House, Boston, London, 2001.
- [3] C.A. Balanis, "Modern Antenna Handbook", John Wiley & Sons, USA, 2008.
- [4] Zhi Ning Chen, Michael Y.W. Chia, "Broadband Planar Antennas Design and Applications", John Wiley & Sons, England, 2006.
- [5] Ahmed El Rabbany, "Introduction to GPS The Global Positioning System", USA, 2002.
- [6] Thomas A. Milligan, "Modern Antenna Design, Second Edition", John Wiley & Sons, New Jersey, 2005.
- [7] "Antenna Polarizations and How They Radiate"
<http://www.mpanntenna.com/what-is-antenna-polarization/>, Last accessed at January 2017
- [8] " What is polarization, and what types of polarization exist?"
<http://www.horiba.com/scientific/products/ellipsometers/ellipsometry-academy/faqs/basic/>, Last accessed at January 2017
- [9] Barsur Rao, Edward Rosario "Spatial Null Steering Microstrip Antenna Array", US20030052825, 2003

[10] Rod B. Waterhouse, “ Design of Probe Fed Stacked Patch Antennas”, IEEE Transactions on Antennas and Propagation, Vol. 47, No. 12, December 1999

[11] Xiaoye Sun, Zhijun Zhang, “Dual-Band Circularly Polarized Stacked Annular-Ring Patch Antenna for GPS Application”, IEEE Antennas And Wireless Propagation Letters, Vol. 10, 2011

[12] W. Rowe, R. B. Waterhouse, A. Nirmalathas, and D. Novak, “Integrated antenna base station design for hybrid fiber radio networks,” presented at *IEEE Int. Topical Meet. Microwave Photon.*, Melbourne, Australia, Nov. 1999

[13] Rod B. Waterhouse, “Stacked Patches Using High and Low Dielectric Constant Material Combinations”, IEEE Transactions On Antennas And Propagation, Vol. 47, No. 12, December 1999

[14] Herscovici, N., "A wide band single layer patch antenna," *IEEE Trans. on Antenna and Propagations*, Vol. 46, No. 4, 471474, April 1998.

[15] J. M. Griffin and J. R. Forrest, "Broadband circular disc microstrip antenna," *Electronics Letter*, Vol. 18, No. 6, 1982.

[16] A.K Bhattacharyya, B.E, M. Tech and R. Garg., "Generalized transmission line model for microstrip patches", IEEE Proceedings, Vol 132, No. 2, April 1985.

[17] A.K Bhattacharyya, "Generalized transmission line model of microstrip patch antennas and some applications", PhD Thesis, Indian Institute of Technology, Kharagpur, India, 1985.

[18] Shen L.C, "Analysis of a Circular Disk Microstrip Antenna", Institution of Electrical Engineers, Proceedings, vol. 126, Dec. 1979, p. 1220-1222.

- [19] I.J. Bahl and P. Bhartia, " Microstrip Antennas", Artech House, 1980
- [20] Mustafa Sancay Kırık, " Design, Analysis, And Implementation Of Circular Disk -Annular Ring (Cdar) Antenna", MS Thesis, Middle East Technical University, 2007
- [21] David M. Pozar, "Microwave Engineering", John Wiley & Sons Inc, 3rd ed., 2005
- [22] "Branchline Couplers"
<https://www.microwaves101.com/encyclopedias/branchline-couplers>, March,3, 2007, Last accessed at February 2017
- [23] Günther Schlegel / Alexander Glas, "Application Note SAW- Components", January,27,2004.
- [24] "GPS Antennas locate, communicate, accelerate RF Design Considerations for u-blox GPS Receivers"
https://www.u-blox.com/sites/default/files/products/documents/GPS-Antenna_AppNote_%28GPS-X-08014%29.pdf?utm_source=en%2Fimages%2Fdownloads%2FProduct_Docs%2FGPS_Antennas_ApplicationNote%28GPS-X-08014%29.pdf, Last accessed at February 2017
- [25] "Radio Receiver Noise Floor"
<http://www.radio-electronics.com/info/rf-technology-design/rf-noise-sensitivity/noise-floor.php>
- [26] "Abracon Corporation"
<http://www.abracon.com/index.php>, Last accessed at March 2017

[27] “Surface Mount 1227.60MHz SAW Filter”

<http://abracon.com/Filters/SAW%20FILTERS/AFS20A20-1227.60-T3.pdf>, Last accessed at March 2017

[28] “Surface Mount 1588.66 MHz SAW Filter”

<http://abracon.com/Filters/SAW%20FILTERS/AFS14A34-1588.66-T3.pdf>, Last accessed at March 2017

[29] “Diplexers”

<https://www.microwaves101.com/encyclopedia/diplexers>, Last accessed at March 2017

[30] “Filters”

<http://ntuemc.tw/upload/file/201102212235523ca26.pdf>, May, 5,2014, Last accessed at April 2017

[31] “PMA-545G1+”

<https://www.minicircuits.com/WebStore/dashboard.html?model=PMA-545G1%2B>, Last accessed at April 2017